Advanced Drug Delivery Reviews xxx (2020) xxx

Contents lists available at ScienceDirect

Advanced Drug Delivery Reviews

journal homepage: www.elsevier.com/locate/addr

Review article

Imaging technology of the lymphatic system

Anna K. Polomska [a], Steven T. Proulx [b,*]

[a] ETH Zürich, Institute of Pharmaceutical Sciences, Vladimir-Prelog Weg 1-5/10, 8093 Zürich, Switzerland
[b] University of Bern, Theodor Kocher Institute, Freiestrasse 1, 3012 Bern, Switzerland

ARTICLE INFO

Article history:
Received 19 May 2020
Received in revised form 16 July 2020
Accepted 31 August 2020
Available online xxxx

Keywords:
Lymphatic system
Lymphatic vessel
Lymph node
Lymphangiography
Lymphscintigraphy
MRI
NIR fluorescence
Tracer
Contractility

ABSTRACT

The lymphatic system plays critical roles in tissue fluid homeostasis and immunity and has been implicated in the development of many different pathologies, ranging from lymphedema, the spread of cancer to chronic inflammation. In this review, we first summarize the state-of-the-art of lymphatic imaging in the clinic and the advantages and disadvantages of these existing techniques. We then detail recent progress on imaging technology, including advancements in tracer design and injection methods, that have allowed visualization of lymphatic vessels with excellent spatial and temporal resolution in preclinical models. Finally, we describe the different approaches to quantifying lymphatic function that are being developed and discuss some emerging topics for lymphatic imaging in the clinic. Continued advancements in lymphatic imaging technology will be critical for the optimization of diagnostic methods for lymphatic disorders and the evaluation of novel therapies targeting the lymphatic system.
© 2020 The Authors. Published by Elsevier B.V. This is an open access article under the CC BY-NC-ND license (http://creativecommons.org/licenses/by-nc-nd/4.0/).

Contents

Abbreviations: ^{18}F-FDG, [18F]fluorodeoxyglucose; AUC, area under the curve; CCD, coupled charged detector; CSF, cerebrospinal fluid; CT, computed tomography; DOTA, dodecane tetraacetic acid; DTPA, diethylenetriamine pentaacetate; FITC, fluorescein isothiocyanate; ECM, extracellular matrix; ICG, indocyanine green; LVA, lymphovenous anastomosis; MRI, magnetic resonance imaging; MRL, magnetic resonance lymphography; NIR, near-infrared; OCT, optical coherence tomography; PEG, polyethylene glycol; PET, positron emission tomography; ROI, region of interest; SLN, sentinel lymph node; SPECT, single-photon emission computed tomography.

* Corresponding author.
E-mail address: steven.proulx@tki.unibe.ch (S.T. Proulx).

https://doi.org/10.1016/j.addr.2020.08.013
0169-409X/© 2020 The Authors. Published by Elsevier B.V. This is an open access article under the CC BY-NC-ND license (http://creativecommons.org/licenses/by-nc-nd/4.0/).

Please cite this article as: A.K. Polomska and S.T. Proulx, Imaging technology of the lymphatic system, Adv. Drug Deliv. Rev., https://doi.org/10.1016/j.addr.2020.08.013

ARTICLE IN PRESS

1. Introduction

After the blood circulation, the lymphatic system is the second vascular system in mammalian species. It fulfils vital functions such as the maintenance of tissue fluid homeostasis, the initiation of immune responses via the drainage of antigens and cells and the uptake of dietary lipids in the intestine. Present in most organs of the body, with the notable exceptions of the brain and bone marrow, the lymphatic system is composed of blind-ended lymphatic capillaries responsible for the uptake of interstitial fluid and proteins and downstream collecting lymphatic vessels that actively transport lymph fluid through a series of lymph nodes to the blood circulation [1].

Imaging techniques for visualization of the lymphatic system are less well developed than those for imaging of blood vessels for two major reasons. First, the lymphatic system is more difficult to "make visible". It is normally not apparent to the naked eye even during surgery and its organization as a one-way transport network means that the entire system cannot be easily visualized with a simple injection. Thus, imaging of lymphatic system is usually performed after interstitial injection (e.g. intradermal, subcutaneous or intramuscular) of tracers, the design of which must take into account several factors to enable efficient uptake by the lymphatic vessels of that specific tissue [2–4]. Second, the importance of the lymphatic system in health and disease has been historically underappreciated. Lymphatic vessels were commonly relegated in the past as simple waste conduits responsible for the uptake of only minor amounts of excess fluid produced within tissues; however, an improved knowledge of basic anatomy and physiology and in our understanding of several diseases has indicated the critical role that this system plays within our body [1,5,6]. Thus, for an increasing number of clinical indications there has emerged a clear need for improved imaging technology to visualize the lymphatic system and quantify its function in both patients and in preclinical models of disease.

In this review, we first summarize the established state-of-the art of lymphatic imaging used in clinics. We then outline the most recent developments in the field of pre-clinical imaging, including the design of novel tracers, methods of tracer delivery and new imaging modalities. Next, we focus on preclinical and clinical imaging protocols for the quantitative assessment of the lymphatic function. Finally, we highlight promising novel lymphatic imaging techniques that are currently being translated into the clinic.

2. State-of-the-art of clinical imaging

Clinical imaging can deliver a variety of relevant information about the morphology and function of the lymphatic vessels and lymph nodes. Therefore, visualization of these lymphatic structures in different parts of the body has been utilized to identify and stage numerous conditions, such as lymphedema, cancer, chronic inflammation, chylous ascites and many others [2]. Moreover, imaging of the lymphatic system can be used pre- or intra-operatively in surgical procedures where lymphatics are involved, for example sentinel lymph node (SLN) mapping and metastatic staging, lymphovenous anastomosis (LVA), lymph node transfer, tumor resection or transplantation. In the initial section of this review we will summarize the established clinical lymphatic imaging techniques and discuss their advantages and limitations Table 1.

2.1. X-ray lymphography

X-ray lymphography is the most conventional technique of lymphatic imaging dating back to the 1960s. In this method, a blue dye (methylene blue) is first injected intradermally into the interdigital space of the foot (transpedal lymphography) or hand, which allows for localization of the lymphatic structures with the naked eye (Fig. 1A). Alternatively, a lymph node can be made visible using another technique, for example through ultrasound (transnodal lymphograpy). After that, the lymphatic structure (lymph vessel or lymph node) is cannulated with an iodinated, oil-soluble X-ray contrast agent, Lipidol, followed by X-ray imaging (fluoroscopy, radiography or computed tomography) [7,8].

The advantage of X-ray lymphography is efficient penetration of the X-ray waves into tissues, which allows for visualization of the deep lymphatic structures, such as thoracic duct and iatrogenic or idiopathic leakage at different locations, such as chylous ascites, chylothorax, chyluria or lymphocele [9–12]. In fact, although in some patients lymphography may itself have a therapeutic effect [12], it is often followed by a direct surgical intervention to embolize the site of the leakage [11]. However, this two-step lymphography technique requires significant time and training of the operator, and constitutes a burden for the patient, since for some procedures (e.g. for intranodal or direct thoracic duct injections) the patient needs to be anesthetized and/or sedated. Therefore, this imaging technique has been predominantly replaced by other, less invasive methods and is currently rarely used in clinics except for imaging of the central lymphatics in certain indications.

2.2. Scintigraphic methods

Lymphoscintigraphy is considered as the "gold standard" in clinical lymphatic imaging. Most commonly, it is applied for diagnosis and staging of lymphedema and for SLN mapping. Approved technetium-99m-labeled (Tc99m) lymphatic-specific tracers, varying in terms of size, are used clinically. Typically, these are ^{99m}Tc-nanocolloidal (5–80 nm diameter) human serum albumin [13,14] in Europe, ^{99m}Tc-sulphur colloid (filtered to a diameter below 100–200 nm) in the US and ^{99m}Tc-antimonium-trisulfide (5–30 nm) in Canada and Australia. Other conjugates have also been used in clinical studies, such as ^{99m}Tc-phytate particles (10–20 nm) [15,16] or ^{99m}Tc-immunoglobulin (around 10 nm) [17], 99mTc-dextran [18] or targeted tracers, such as 99mTc-tilmanocept [19–22] or 99mTc-rituximab [23,24].

For functional imaging of the lymphatic system, tracers of small size are preferred to assure a rapid uptake from the injection site into the lymphatic vessels [25]. A general protocol for assessing lymphatic function with lymphoscintigraphy involves interstitial (intradermal or subcutaneous) injection of a radioactively labeled tracer in the interdigital space of both healthy and lymphedemous hands or feet and static or dynamic imaging of the limbs, or occasionally the whole body, with a gamma camera (posterior or anterior) to obtain an image of the lymphatic structures (Fig. 1B). Although the acquired images are typically low resolution, their qualitative analysis provides descriptive information about the symmetry of the tracer uptake in the lymphatics and lymph nodes of the healthy and lymphedemous limb as well as presence of dermal backflow [16,26]. On the other hand, quantitative or

Please cite this article as: A.K. Polomska and S.T. Proulx, Imaging technology of the lymphatic system, Adv. Drug Deliv. Rev., https://doi.org/10.1016/j.addr.2020.08.013

Table 1
State-of-the art clinical imaging of the lymphatic vasculature.

Technique	Typical tracers	Applications	Advantages	Limitations	Depth limitation	Resolution
X-ray Lymphography	Lipidol	Visualization of the central lymphatic system	Deep penetration of the X-ray waves into the tissues	Invasiveness (need for cannulation of lymphatic vessels or intranodal injection)	No limit	~1 mm
Lymphoscintigraphy	99mTc-coupled radioactive probes	Quantitative assessment of lymphatic function, imaging of collecting lymphatic vessels, visualization of dermal backflow, SLN mapping	Deep penetration of gamma waves, high sensitivity	Exposure to ionizing radiation, poor spatial and temporal resolution, planar image, lack of standardization	No limit	~1.5 cm
SPECT/CT	99mTc-coupled radioactive probes	SLN mapping, assessment of the status of the lymphatic vessels	Tomographic reconstruction to create a 3D image displaying the localization of the radioactive signal in relation to other tissues	Exposure to ionizing radiation, poor spatial and temporal resolution, high costs	No limit	1–2 cm for SPECT / ~50–200 μm for CT
NIR lymphography	ICG	Quantitative assessment of lymphatic function, imaging of collecting lymphatic vessels, visualization of dermal backflow pattern, SLN mapping	Lack of exposure to ionizing radiation, better spatial and temporal resolution than scintigraphy, low costs	Limited depth of imaging, lack of appropriate clinically-approved tracers for quantitative imaging	1.5 cm	Dependent on imaging depth and instrumentation (typically in the μm range)
MR lymphography	Gd-based tracers or iron oxide	Functional (MR dynamic lymphography) and morphological evaluation of lymphatic vessel status, SLN mapping, imaging of central lymphatics	Lack of exposure to ionizing radiation, high imaging depth limit, 3D volumetric images of the lymphatic vessels can be obtained	Low lymphatic specificity of clinically-approved tracers (higher specificity can be obtained during intranodal injection), venous signal enhancement, high costs	No limit	0.5–2 mm

semi-quantitative approaches for assessing the lymph transport, such as measuring the disappearance of the tracer at the injection site after interstitial administration [27], the kinetics of proximal lymph node uptake [13] or a quantification of the asymmetry of the tracer uptake in the limbs have been published [28]. It is important to note that in quantitative studies using lymphoscintigraphy the results need to be corrected for the radioactive decay of the tracer itself.

Lymphoscintigraphy is also widely used for SLN mapping after interstitial (e.g. intradermal, intratumoral or interareolar) injection of radioactive tracers in several types of cancer [20,29]. After administration, lymphoscintigraphic imaging is performed to localize the SLNs using gamma cameras or intraoperatively using a portable gamma probe that gives an acoustic signal upon detection of radioactivity. Newer portable gamma-cameras are being developed that are combined with optical imaging to provide anatomical location of the SLN using blue dye or indocyanine green to provide a visual discrimination of the boundary to finely guide surgical dissection [29–31]. An ideal tracer for SLN mapping should exhibit rapid clearance from the injection site, rapid accumulation and high retention in the SLN as well as low accumulation in the downstream lymph nodes [25]. In the US, 99mTc-sulphur nanocolloid is typically used for this purpose; however, due to its large size it is slowly cleared from the injection site [32]. To overcome these issues, targeted approaches have been developed. 99mTc-tilmanocept (Lymphoseek, Navidea) is an FDA-approved lymphoscintographic agent composed of 99m-Tc bound DTPA-mannosyl dextran, a macromolecule of size around 7 nm and 99mTc-rituximab, containing 99mTc coupled to a monoclonal antibody. Both tilmanocept and rituximab target cells residing in the lymph nodes: the former acts as a ligand for the CD206 receptor on macrophages and dendritic cells and the latter for CD20 on the surface of B-lymphocytes, thus limiting the migration of the tracers into downstream lymph nodes [20,22].

Classical lymphoscintigraphy delivers only planar images and fails to provide information about the accurate anatomical location of the lymphatic abnormalities or lymph nodes within the tissue. To address this shortcoming, SPECT/CT imaging can be performed [33] where scintigraphic imaging with a specialized gamma camera is combined with X-ray tomography. In particular, during the measurements, the 2D images are recorded by detectors placed at different angles, followed by a tomographic computer-assisted reconstruction to create a 3D image displaying the localization of the radioactive signal in relation to other tissues. Typically, SPECT/CT is used for precise, pre-operative SLN mapping in multiple types of cancers to assist surgical planning [34–38]. Like in classical lymphoscintigraphy, 99m-Tc-based probes are used in clinical SPECT/CT imaging.

Currently, the technical aspects of protocols for scintigraphic methods for staging and diagnosis of lymphatic insufficiencies and SLN mapping vary among different medical centers worldwide in terms of use of the tracer type, the injection route, the application of stress activity to stimulate lymphatic uptake (e.g. applying temperature, limb exercise) and the data analysis methods. This is a major obstacle to compare the findings across different studies [26,29]. Other limitations of lymphoscintigraphy are related to its poor spatial and temporal resolution as well as the need to use large, stationary and expensive instrumentation. The costs of production and disposal and the short radioactive half-life of such tracers are also of high concern. These issues are likely to hamper any major breakthroughs in the lymphoscintigraphy field in the coming years [26].

2.3. Fluorescence imaging

Fluorescence microlymphography is a useful "office" test to visualize the initial capillary lymphatic network localized in the dermis of the skin. In this technique, which was originally developed in the early 1980s, FITC-dextran (150 kDa) is injected intradermally [39]. The fluorescent tracer spread into the initial lymphatics is visualized with a microscope and is measured as the maximum distance from the outer border of the dye deposit. More extensive spread of the tracer suggests lack of drainage into the deeper lymphatic collecting vessels implying their impairment. A cut-off of 12 mm spread has been shown to distinguish between healthy and lymphedema legs in patients with high sensitivity and specificity [40–42]. However, this technique has been scarcely adopted in the lymphology field, since FITC-dextran, although well-tolerated in patients, is not officially approved for human use.

Near-infrared (NIR) lymphography is a relatively new technique that has been first used in humans around 15 years ago [43–46]. In NIR lymphography, the clinically-approved dye indocyanine green

Please cite this article as: A.K. Polomska and S.T. Proulx, Imaging technology of the lymphatic system, Adv. Drug Deliv. Rev., https://doi.org/10.1016/j.addr.2020.08.013

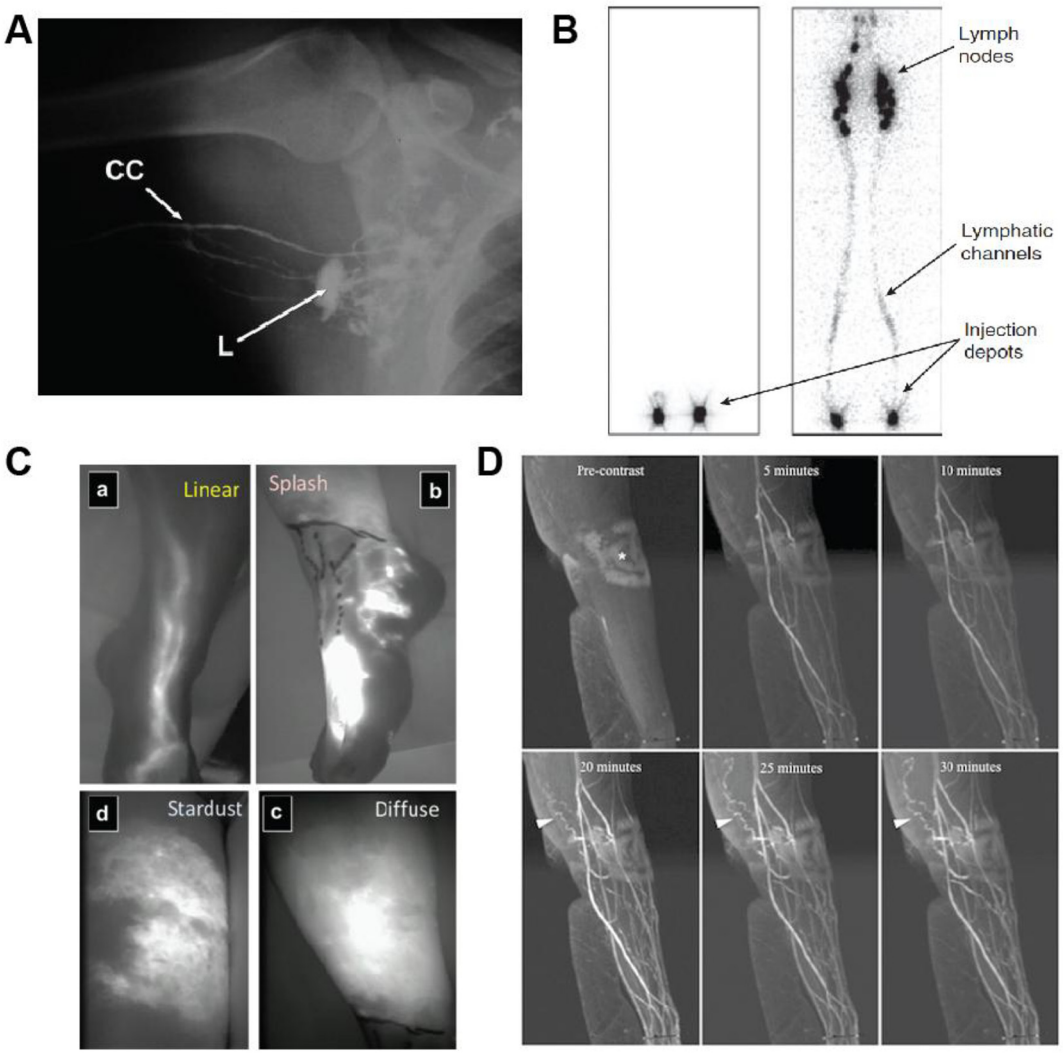

Fig. 1. State-of-the-art clinical imaging of the lymphatic system with tracer-based techniques. (A) X-ray lymphography. Radiographic image during axillary lymph node mapping with Lipidol. In the left image, three larger afferent lymphatic collectors of the upper extremity are shown. Collectors (CC) are directed to larger, laterally-localized axillary lymph node (L). Reproduced with permission [8]. (B) Lymphoscintigraphy. Lymphoscintigrams of the legs after subcutaneous injection of radioactive tracers in the feet (foot depots marked with the arrows). Left image shows minimal lymphatic uptake in legs of patient with primary unilateral lymphedema. Right image shows the lymphatic routes and inguinal lymph nodes imaged in normal control individual. Reproduced with permission [42]. (C) NIR lymphography. Dermal backflow patterns that correlate to severity of lymphedema and lymphatic dysfunction in comparison to normal linear flow pattern (left). In extreme cases of no flow, the tracers may not extend beyond the injection site. Reprinted with permission [55]. (D) Dynamic MR lymphography with Gd-based tracer in the upper arm with lymphedema. Progressive enhancement of the lymphatic channels over time. Irregular radiating lymphatic channels are seen extending from the lateral forearm towards the medial left elbow in a characteristic irregular, beaded pattern (arrowheads). Reprinted with permission [66].

(ICG) is injected intradermally near the area of interest and the region of interest (ROI) is imaged using a coupled-charged detector (CCD) camera. ICG was originally FDA approved in 1959 for use in hepatic clearance assessments and was later adapted for use in measurements of cardiac output and ophthalmologic angiography. ICG has been widely reported to bind serum albumin in vivo, however, studies have shown that it binds even more strongly to HDL and LDL lipoproteins [47]. In pioneering studies, the feasibility of visualizing abnormal lymphatic architecture and lymph flow velocities in patients with secondary arm lymphedema using this technique was shown [44,45]. Owing to high light penetration and low scattering of light in the NIR range, this technique is capable of visualizing lymphatic structures up to 2 cm below the skin using an ICG dose in the microgram range. Owing to improved spatial and temporal resolution in comparison to lymphoscintigraphy, NIR lymphography opens a variety of opportunities for precise delineation of lymphatic architecture and quantitative assessment of function such as measurements of collecting vessels contractility [44,48–51]. For example, while with radioactive lymphoscintigraphy dermal backflow can be evaluated only in terms of presence or absence, NIR lymphography allows for observation of distinct dermal backflow patterns (splash, stardust and diffuse) that are correlated to the severity of lymphatic dysfunction and clinical symptoms (Fig. 1C) [52–55].

NIR lymphography has also been clinically useful in evaluating the lymphatic flow in transplants (i.e. hand transplants, free flap transplants or vascularized lymph node transfer) [56,57], for identification of lymphatic vessels prior to LVA surgery [58,59] and during SLN mapping in cancer patients [60]. Although for the latter application ICG is not ideal due to its low molecular weight, resulting in its poor retention in the SLN and leakage into the surgical field, it has been shown to be clinically useful to detect SLNs in many types of cancer (breast cancer, gynecological cancers, melanoma, head and neck cancer) often in combination with modern intraoperative imaging equipment [61–65]. An advantage of using ICG in SLN mapping is the possibility of real-time tracking of the lymph flow from the injection site to the SLN [61].

Despite the widespread use of ICG in the field of lymphatic imaging, this indication, including all injection routes other than intravenous, remains off-label. Moreover, the undesirable physicochemical properties of ICG, such as poor stability, self-quenching and low quantum yield,

Please cite this article as: A.K. Polomska and S.T. Proulx, Imaging technology of the lymphatic system, Adv. Drug Deliv. Rev., https://doi.org/10.1016/j.addr.2020.08.013

currently limit the full potential of the NIR lymphography technique [67]. Thus, there is a clear need for clinically approved tracers for this imaging modality that are optimized for the lymphatic system.

2.4. Magnetic resonance imaging

Magnetic resonance lymphography (MRL) imaging in the extremities is performed after interstitial injection of a T1-weighted Gd-based contrast agent (typically Gd-DTPA or Gd-DOTA) that creates a desirable positive enhancement signal. Owing to the high imaging depth of MRI, 3D volumetric images of the lymphatic vasculature can be obtained. In particular, the location (including the depth) of dilated, tortuous lymphatics as well as the location and extent of dermal backflow can be identified. The vessels can be visualized in relation to other anatomical structures and/or pathological changes resulting from lymphedema (i.e. fibrotic and adipose tissue accumulation or subcutis thickening) obtained from 3D T2-weighted pre-tracer imaging [66,68]. In addition to staging of lymphedema, MRL is especially useful in pre-operative imaging prior to LVA surgery, in contrast to NIR lymphography, as its large field of view allows for imaging of the whole extremity and for spatial localization of the lymphatic and blood vessels within the healthy and pathological structures, which facilitates the choice of the proper vessels for the anastomosis [69–71].

Due to the low molecular weight of clinically utilized Gd-based tracers (<1 kDa), after interstitial injection the contrast agent is absorbed not only by the lymphatics but also by the blood vascular system, which lowers the specificity of this imaging technique [72]. Lymphatic vessels may be distinguished from the blood vessels based on their anatomical structure but they are sometimes not easy to delineate. Another approach is to acquire a series of dynamic images and to distinguish lymphatic vessels as the vessels in which the tracer signal increases and then slowly decays and blood vessels as those where the signal enhancement decreases over time (Fig. 1D) [66,73]. As these data are still often difficult to interpret, a second MRI imaging step after intravenous injection of the same contrast agent ("delayed MR lymphogram") can be performed in order to distinguish the lymphatic and blood vasculature [68].

Dynamic MRL allows for imaging of the central lymphatic system (i.e. thoracic duct and cisterna chyli) or hepatic lymphatics and it is a modern, emerging alternative to X-ray lymphography [74,75]. Similar to this historical technique, the Gd-based tracer (Gd-DTPA or Gd-DOTA) is usually injected intranodally with the support of ultrasonography to enable direct transport of the contrast agent to the central lymphatics followed by T1-weighted sequences [75,76]. Intranodal injection of the tracers in combination with dynamic MRL seem to improve the lymphatic specificity [76]. Moreover, recently central lymphatics were also successfully visualized in patients using a transpedal MRL approach [77].

Non-contrast MRI lymphography sequences have been used for imaging of the central lymphatic system and lymphedema. The use of heavily T2-weighted sequences for the imaging allows for highlighting the signal from the stagnant fluid in the lymphatic vessels and in the tissue, while depressing the signal from the tissue itself, thus depicting the localization of the limb edema or the leak in the central lymphatics [78–81]. The presence of the stagnated fluid within the fat tissue helps to confirm the lymphatic origin of the swelling, as opposed to venous origin [82]. In addition, as for MRL, the non-contrast MRI can visualize the anatomical changes of the tissues affected by lymphedema [79].

However, non-contrast MRI is capable to visualize lymphatic vessels only when they become dilated and filled with stagnant fluid. Along this line, the method is not suitable for dynamic flow analysis. For this purpose, arterial spin labeling MRI, conventionally used to quantify blood flow and tissue perfusion, can be applied to measure the lymphatic flow velocity [83]. Another tracer-free MRI-based technique is chemical exchange saturation transfer (CEST) MRI. In this method the contrast originates from the protons associated with amide groups in endogenous proteins, which makes it sensitive to the protein-rich interstitial environment. The accumulation the protein-rich interstitial fluid is an indirect indication of lymphatic dysfunction, e.g., in lymphedema [84,85]. The advantage of non-contrast MRI is its non-invasiveness and reduced time of imaging compared to MRL resulting in lower costs and a decreased risk of allergic reactions. However, the resolution of this technique MRI remains poor. Moreover, further investigations in larger groups of patients are necessary to validate its clinical utility.

The major advantage of MRI in contrast to X-ray lymphography is that patients are not exposed to ionizing radiation. Lymphatic structures can be visualized with a resolution higher than in lymphoscintigraphy and NIR lymphography within the 3D volumetric structure of the surrounding tissues when contrast agent is used. The major limitations of MRI remain high costs of instrumentation and the advanced technical skills required to operate the equipment and interpret the data. Moreover, the lack of appropriate clinically-approved lymphatic-specific MRI tracers has hampered the utility of this imaging technique.

3. Technological advancements in preclinical lymphatic imaging

In vivo imaging of the lymphatic system in animal models has made great strides in the past 15 years. Traditionally, in experimental studies, lymphatics were visualized through tissue injections of ink or vital dyes, such as Evans blue, that enabled the normally transparent vessels to be visible during surgical manipulations or in thin skin preparations such as the mouse ear [86–88]. However, advancements in tracer design and imaging technology has enabled functional imaging of lymphatic vessels in vivo at high temporal and spatial resolution, allowing an array of techniques utilizing different imaging modalities to be developed. While some imaging approaches were adapted from existing clinical techniques, such as MRI and NIR fluorescence imaging, promising new modalities have also been introduced such as optoacoustic and optical coherence tomography (OCT). In this section, we will highlight advancements in tracer design and delivery and describe by imaging modality some of the recent innovations in preclinical lymphatic imaging.

3.1. Tracer design and delivery

3.1.1. Size

Small-sized molecules (typically of size <5 nm diameter or below 10 kDa for proteins or polymers) diffuse rapidly in the interstitium and can permeate to both blood and lymphatic capillaries [89,90]. Blood flow is approximately 100–500 times faster than lymph flow within tissues, resulting in preferential clearance of small molecules via blood capillaries. Due to the direction of the convective flow in the interstitium from the blood to lymphatic vessels and discontinuous button-like junctions between endothelial cells in lymphatic capillaries, larger tracers are preferentially cleared via this route. For example, in our recent study we encapsulated ICG in micelles of around 12 nm consisting of Kolliphor HS15 (polyoxyl 15 hydroxystearate). After intradermal injection of ICG-Kolliphor HS15 solution into the dorsal aspect of the mouse foot, the tracer could be visualized only in the popliteal collecting lymphatic vessels as opposed to free ICG, which was evident also in veins draining the injection site [91]. It is generally agreed that tracers within the size range of 10–100 nm are suitable for lymphatic imaging and that their uptake rate from the injection site is size dependent [92,93]. For example, Zbyszynski et al., investigated the clearance of the sulfo-Cy5-labeled PEGylated functional upstream domain peptide from the subcutaneous injection site in mice. The clearance half-life for 10–40 kDa conjugates was directly proportional to the molecular weight of the PEG [92]. Similar results were obtained for FITC-labeled dextrans in the size range of 5–54 nm. After intradermal injection, the skin dye-polymer exposure over 72 h, as quantified by an AUC assessment, increased with increasing molecular weight of dextran, with an opposite effect found for lymph node exposure, indicating a retention

Please cite this article as: A.K. Polomska and S.T. Proulx, Imaging technology of the lymphatic system, Adv. Drug Deliv. Rev., https://doi.org/10.1016/j.addr.2020.08.013

of the larger-sized molecules at the injection site and thus their reduced transport to the lymph nodes [93]. Above 100 nm, the diffusion of the entities in the interstitium and thus entry into the lymphatics is thought to be limited by the size of the conduits in the extracellular matrix (ECM) [25,94].

The exact choice of the tracer size depends on the application. For example, tracers for lymphatic flow imaging should in principle be smaller (5–10 nm) to allow for rapid lymphatic uptake and visualization. On the other hand, the tracers for lymph node imaging should have an intermediate size (10–100 nm) in order to accumulate in this organ and thus provide strong signal [3,25,94–97]. For example, DSouza et al., quantitatively visualized the lymphatic vessels and lymph nodes after interstitial injection of two fluorescent tracers of different molecular weights, namely methylene blue (ca. 300 Da) and a fluorophore-conjugated IgG (ca. 66.5 kDa) in the mouse hindlimb. Importantly, the active lymphatic pumping was not affected by the molecular weight of the tracer, as opposed to the passive diffusion affecting the uptake by the lymphatics, which was reflected by the delayed time of reaching the fluorescence peak in the afferent lymphatic vessel after injection of the IgG and the higher signal compared to methylene blue [98]. There is no consensus in the literature concerning the "ideal" size of the tracer for the SLN mapping. Many researchers claim it to be below 50 nm, due to optimal balance between retention at the injection site and at the lymph node [25]. However, Yang et al., investigated in mice a series of self-assembled NIR fluorescent nanoparticles composed of amphiphilic perylene diimide in the size range 50–200 nm for SLN imaging using optoacoustic imaging. The optimal size of nanoparticles for SLN imaging was found to be 100 nm due to 60 min interval in the arrival time between investigated lymph nodes (popliteal and sciatic) after local administration [96].

Many conventional tracers used currently in clinical lymphatic imaging, such as the MRI tracers Gd-DTPA or Gd-DOTA, isosulfan or ICG dye, are of low molecular weight which limits their lymphatic specificity. Therefore, a number of researchers use strategies like encapsulation of tracer in nanoparticles such as liposomes [99,100], calcium phosphate particles [101] or micelles [91], pre-complexation with polymers [102] or proteins [103] or covalently attaching larger molecules (e.g. PEG) [90,104–106]) to obtain lymphatic-specific tracers of larger size. For example, Bisso et al., developed PEG-stabilized calcium phosphate nanoparticles (150 nm) loaded with MRI contrast agent, Gd-DTPA. Intradermally injected nanoparticles exhibited slower uptake kinetics in the popliteal lymph node and the MRI signal intensity exhibited lower variability compared to free Gd-DTPA. A defined and reproducible kinetic pattern would be an advantage in quantitative assessments of lymphatic dysfunction [101].

3.1.2. Surface charge/properties

Negatively charged hyaluronic acid is one of the major components of the ECM. Thus, negatively charged probes are preferred for in vivo imaging applications due to their lack of interactions within the ECM that hinder their clearance from the interstitium and uptake by the lymphatic capillaries [107]. However, small particulate-based tracers with only a slight negative charge have the tendency to aggregate upon injection in the interstitium. For example, negatively charged silica particles with size 35–45 nm doped with Cy7 NIR fluorescent dye were investigated in mice for lymph node mapping. When the negatively charged carboxylic groups were exposed on the surface, the particles were transported very slowly to the lymph node, presumably due to aggregation at the injection site. On the other hand, when the carboxylic acid groups were masked with PEG and buried within the core of the particles, particles were transported rapidly to the lymph nodes, reaching the peak fluorescence signal within minutes after injection [108]. Aggregation could also be a reason for the lack of size-dependency of skin retention and lymph node accumulation of small polystyrene particles injected intradermally in mice [93]. In another study, negatively charged G4-G8 carboxy-terminal dendrimers were cleared from the injection site and then detected at the lymph node, while the same generation of amino-terminal dendrimers were stuck in the interstitium. Interestingly, slightly negatively charged G4-G8 acetyl-terminal dendrimers exhibited diffusion into the blood despite their larger molecular weight [89].

However, in some cases, positively charged species can also be efficiently cleared from the injection site. For example, 100 nm positively charged poly-arginine capsules accumulated to a higher extent in the popliteal lymph node of mice after intradermal injection in comparison to negatively charged anionic carboxymethyl-beta-glucane and chitosan capsules of similar size. It is possible that certain positively charged polymers, such as poly(arginine), may confer special properties to the surface of the tracer that could alter their interactions with the endogenous soluble proteins and small molecules, forming a "corona" on the surface of the nanocarriers. This may alter their interactions with the ECM and thus uptake by the lymphatics [109]. If cleared efficiently from the injection site, positively charged tracers would be indeed beneficial for lymph node imaging, as they tend to accumulate at this site due to uptake by the immune cells. It needs to be investigated in more detail how the protein corona influences the interactions and retention within the interstitium and lymph node. Interestingly, potential specific binding of the probe to interstitial proteins appears to have little influence on the retention of the probe at the injection site, unlike the effect of probe size. Replacing the fibronectin-binding peptide (FUD) in a FUD-sulfo-Cy5-PEG conjugate with its non-binding version (mFUD) had no significant influence on the clearance half-life for any of the PEG conjugates [92].

3.1.3. Tracer delivery

Lymphatic-specific tracers are usually delivered using conventional injection techniques into the interstitium (e.g. through intradermal, subcutaneous, intramuscular or intratumoral routes) from where they reach the lymphatic vasculature. Among these delivery routes, intradermal injection is preferred due to its accessibility and the high interstitial pressure generated by the dense collagen matrix, driving the rapid uptake of the injected tracer into the initial lymphatics [17]. However, intradermal injection using conventional Mantoux technique requires specialized training and may create discomfort and pain [110].

Microneedle-based delivery has been attracting a lot of attention not only in the context of drug and vaccine delivery [111,112] but also for diagnostic and monitoring applications [113]. Microneedles allow for a pain-free and precise delivery of the tracer to a specific depth in the skin dermis. For example, we embedded ICG in 400 μm-long solid polymeric microneedles composed of poly(N-vinylpyrrolidone). After application on mouse skin, the polymer matrix dissolved thus releasing the tracer. These needles allowed for qualitative imaging of the leg lymphatic vessels as well as for quantitative assessments of lymphatic clearance in mouse ears based on disappearance of the tracer from the injection site [102]. However, the low quantity of delivered ICG and poor mechanical stability of the microneedles constitutes their major limitations. Therefore, in our recent work, we used 600 μm-long solid hollow microneedle-based devices, MicronJet600™ (Nanopass Ltd), to deliver micellar ICG solutions into pig skin [91]. These CE-certified devices consist of three hollow pyramidal-shaped silicon crystal microneedles embedded on the plastic base and are compatible with standard syringes. Thus, they can be easily implemented into clinical settings [114]. Kwon et al., have developed an interesting intradermal delivery system, SOFUSA™, consisting of a hollow 350 μm-long silicon microneedle array with nanotopographical polymer film on the surface, attached to a syringe pump. Although the system was developed for the delivery of immunotherapy to the lymph nodes, it is also suited for imaging applications. Namely, the authors have shown that the lymph nodes could be successfully visualized in vivo in rats and in humans after delivery of ICG with SOFUSA [115].

Please cite this article as: A.K. Polomska and S.T. Proulx, Imaging technology of the lymphatic system, Adv. Drug Deliv. Rev., https://doi.org/10.1016/j.addr.2020.08.013

3.2. Developments in preclinical lymphatic imaging

3.2.1. MRI

MRI has been employed for over 20 years for preclinical lymphatic imaging applications. Early work was primarily focused on the development of macromolecular contrast agents that would enable visualization of lymph nodes, of interest for image-guided mapping of SLNs (as reviewed in Misselwitz [116]). These studies have centered on formulations of Gd-based contrast agents that could be administered into interstitial tissue for subsequent lymphatic transport and visualization of draining lymph nodes [117–120]. While some agents did show great promise for this application, potential concerns regarding the toxicity of Gd-based contrast agents have prevented macromolecular-based MR contrast agents from reaching the clinic.

While the high costs and advanced technical knowledge necessary to operate MRI have limited the application of this technique for preclinical lymphatic studies, the developed Gd-based contrast agents have found some utility for basic research. The group of Alana Ruddell has performed a series of studies using dynamic MRI assessing the effects of melanoma tumor growth and metastasis on lymph flow in mice [121–123]. The authors compared three different Gd contrast agents for tumor-draining lymph node detection and found that a 75 nm lipid nanoparticle exhibited the best uptake into inguinal lymph nodes in mice [123]. The authors speculated that the remodeling of the lymph node that occurs in response to the tumor may improve the barrier function of the lymph node to improve retention of nanoparticles. Supporting this hypothesis, less nanoparticles were found in downstream second-tier nodes of tumor-draining lymph nodes compared to uninvolved lymph nodes. The mechanism of this improved retention still remains to be elucidated but may have significance for the delivery of immunotherapy to tumor-draining lymph nodes.

Müller et al., utilized AGuIX, sub-5 nm nanoparticles composed of a polysiloxane core and gadolinium chelates, and 9.4 Tesla MRI for the investigation of lymphatic drainage in a rat hindlimb lymphedema model [124]. In healthy animals, these methods allowed excellent anatomical visualization of lymphatic vessels and lymph nodes with high signal-to-noise ratios (Fig. 2A). After lymphadenectomy of the popliteal lymph node, the imaging revealed lymphatic rerouting through collateral lymphatic vessels that peaked at 6 weeks and gradually subsided over time.

Recently, there has been a renewed interest in imaging the lymphatic drainage of cerebrospinal fluid (CSF), a process long-thought to occur directly to veins [125,126]. Several groups have begun to employ MRI to visualize this process after injection of Gd-based contrast agents into the CSF space in rats and mice [127–130]. Dynamic contrast-enhanced MRI techniques have visualized the distribution of the contrast agents within the CSF and mapped the outflow routes to cranial-draining lymph nodes in the cervical region. We have also recently utilized MRI with a 17 kDa dendritic Gd-based contrast agent, Gadospin D, in conjunction with fluorescence imaging to characterize the CSF outflow routes from the spine to the sacral and deep iliac lymph nodes [131]. Alterations in the lymphatic drainage of CSF and, by extension, the immunosurveillance of the CNS, have been implicated in several conditions including aging and neurodegeneration, multiple sclerosis and glioblastoma [132–135]. Advanced MRI quantifications of the CSF clearance process to lymphatics are being developed and will be critical for the assessment of novel drug formulations for these conditions.

3.2.2. et PET

PET has limited utility for lymphatic vessel imaging in small animal models due to issues of poor resolution, high equipment costs and the need for radioisotopes. Nonetheless, because of its high sensitivity and excellent depth penetration through the whole animal, it has been successfully applied for detection of lymph nodes in rodents, as demonstrated in the following studies.

A targeted immuno-PET approach was developed by Mumprecht et al., to allow sensitive visualization of lymph nodes undergoing lymphangiogenesis, an early stage biomarker for tumor metastasis in several types of cancer [136]. Utilizing intravenous injections of antibodies specific for a lymphatic vessel marker, LYVE-1, the authors were able to demonstrate enrichment of the radioiodinated PET probe in melanoma-draining lymph nodes in mice. Imaging of metastasis in the draining lymph nodes using this probe was found to be more sensitive compared to the [18F]fluorodeoxyglucose (^{18}F-FDG) PET commonly utilized in the clinic.

Thorek and colleagues utilized PET in conjunction with CT and MRI for 3D visualization of draining lymph nodes in mice [137,138]. In an initial study, the authors injected ^{18}F-FDG intradermally in the tail and were able to visualize the sacral and deep iliac lymph node groups enhancing with the tracer (Fig. 2B). Activity curves over time were generated allowing quantification of the tracer uptake into the different lymph nodes [137]. However, the rapid clearance into the blood of this small molecular weight probe is a limitation. In a second study, this group introduced a multi-modal nanoparticle, ^{89}Zr-ferumoxytol, of 17–35 nm in diameter that allowed PET/MRI detection of lymph nodes after administration in the forepaw or to the prostate of mice [138]. While concurrent anatomical visualization of lymph nodes with MRI is a desirable feature, the negative contrast generated by this iron oxide-based contrast agent is a drawback.

Another group has developed a tri-modal PET probe using ^{64}Cu silica nanoparticles that can be used for lymph node detection with fluorescence imaging using a NIR dye and MRI using Gd^{+3} chelation [139]. In a tumor model, the authors compared the detection of the SLN between the three different imaging modalities over the course of several days. This comparison revealed the low sensitivity of the MRI to detect the probe as well as the loss of the PET signal due to the short radioactive half-life of ^{64}Cu. This group has also developed a small molecular weight ^{18}F PET probe conjugated with Evans blue dye, which takes advantage of the inherent property of this dye to bind albumin in the interstitial space [140]. This approach is more favorable from a biosafety standpoint. As Evans blue dye has both visible and fluorescence properties, the authors propose that such a tracer may also be used during surgery.

3.2.3. Fluorescence imaging

The recent development of methods for preclinical imaging of the lymphatic system has largely centered on fluorescence imaging due to its cost-effectiveness, superior resolution, and lack of radiation exposure. Pioneering studies from the group of Rakesh Jain adapted the fluorescent microlymphangiography technique originally developed for use in human skin for lymphatic imaging in the mouse tail [39,141]. Imaging in the tail with FITC-dextran was then extended to studies of lymphedema induced after a circumferential wound and to lymphatic vessels near tumors using a murine sarcoma implanted under the tail skin [142,143]. Dextran dyes were further utilized to image tumor-associated lymphatic vessels using multiphoton microscopy of the tail [144], within window chambers in the flank [145] and of the mouse ear [146].

Fluorescent dextrans were also utilized to demonstrate altered lymphatic morphology in transgenic mouse models, including hyperplasia of the lymphatic vessels in the tail and ear skin of K14-VEGF-C and -D mice [147,148] and abnormal developing collecting lymphatic vessels in Foxc2$^{-/-}$ mice [149]. However, the development of lymphatic-specific fluorescent reporter mice has allowed for the visualization of lymphatic morphology in a tracer-free manner. A number of these mice expressing fluorescent proteins under lymphatic promoters such as Prox1 and VEGFR-3 have now been generated [150–154] and have gained widespread use in the lymphatic research community. Novel high-resolution 3D imaging approaches to visualize the lymphatic vessels in these reporter mice embryos has shed new light on the beginning stages of lymphatic development [155,156]. A related approach using bioluminescent reporter mice expressing firefly luciferase under the

Please cite this article as: A.K. Polomska and S.T. Proulx, Imaging technology of the lymphatic system, Adv. Drug Deliv. Rev., https://doi.org/10.1016/j.addr.2020.08.013

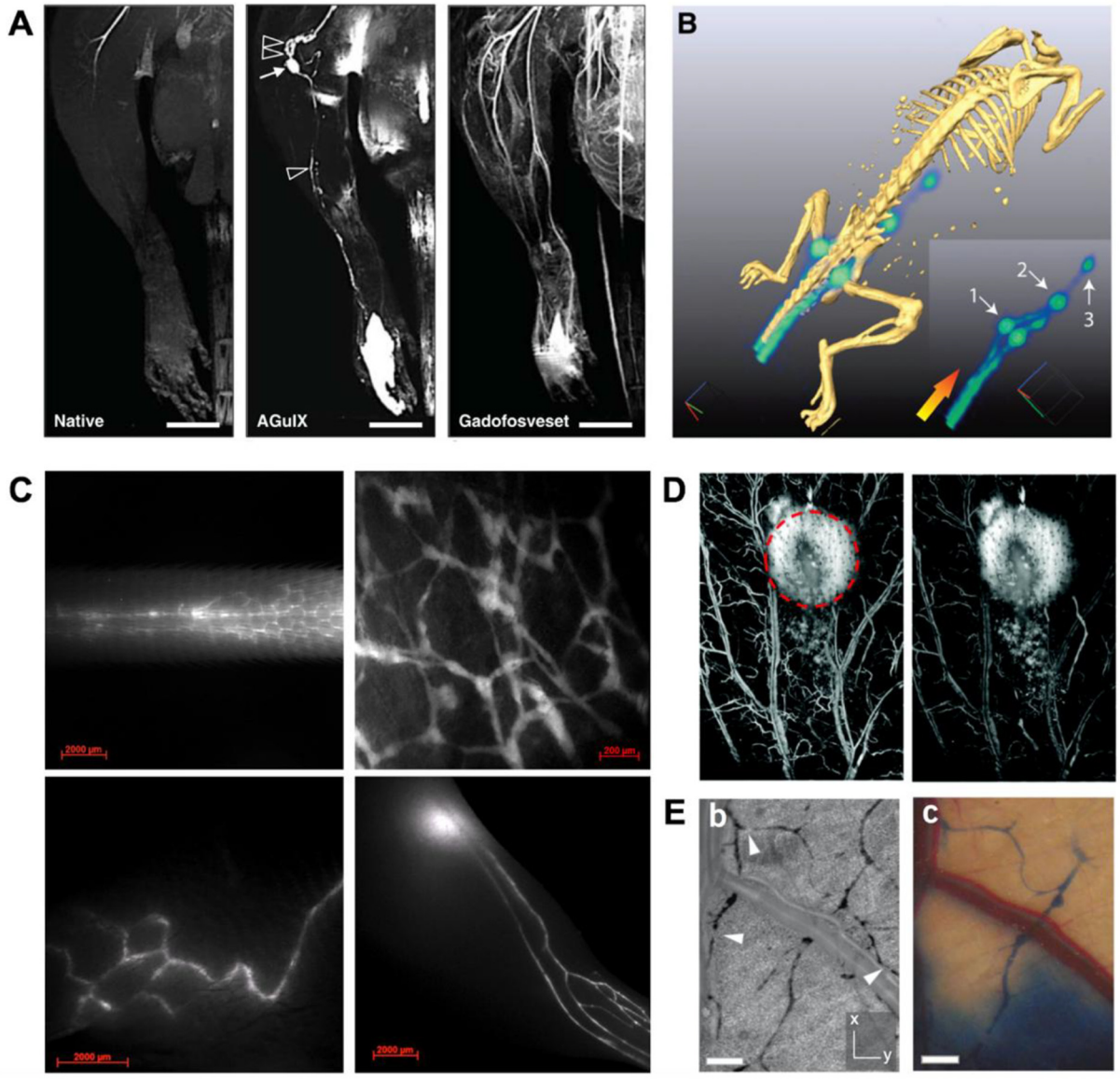

Fig. 2. Overview of preclinical lymphatic imaging modalities. (A) MRI scan of rat hind limb before (left) and after (middle) intradermal injection of AGuIX nanoparticles of 3 nm diameter. Collecting lymphatic vessels (arrowheads) draining to and from the popliteal lymph node (arrow) can be visualized. Intravenous gadofosveset injection (right) was performed 2 h after AGuIX application for simultaneous visualization of blood vessels. Reproduced with permission from [124] (B) Three-dimensional PET/CT rendering of lymphatic system draining the mouse tail after intradermal administration of 18F-FDG (insert is without fused CT). Lymphatic vessels in the tail leading to sacral nodes (1), caudal (2) and mesenteric nodes (3) can be clearly visualized. Reproduced from [137]. (C) NIR visualization of lymphatic vessels after intradermal injection of PEGylated fluorescent tracers in C57BL/6 albino mice. Images acquired with a NIR stereomicroscope of the tail (upper left), ear skin (upper right), flank skin (lower left) and hind limb with popliteal lymph node (lower right) are shown. Reproduced with permission from [90]. (D) Photoacoustic microscopic images of a mouse ear at 560 nm (left) and 595 nm (right) after intradermal injection of 3% Evans blue dye. Blood vessels are visualized through hemoglobin detection at both wavelengths while dye-filled lymphatic vessels are more apparent at 595 nm. Reproduced from [184]. (E) Optical coherence tomography technique for visualization of lymphatic vessels in the mouse dorsal skin. Through negative scattering, lymphatic vessels are apparent as empty spaces within the tissue (b). Lymphatic valves are also apparent (white arrowheads). OCT allows visualization of more lymphatic vessels compared to traditional Evans blue lymphangiography (c) Reproduced with permission from [189]. (For interpretation of the references to colour in this figure legend, the reader is referred to the web version of this article.)

VEGFR-3 promoter has provided a non-invasive method to quantify lymphangiogenesis in inflammation and tumor models [157].

Fluorescence imaging in the visible wavelengths (400 to 700 nm) is limited due to high absorption of photons by endogenous tissue constituents. Additionally, significant tissue autofluorescence in this range also increases the background signal that is obtained. To address these limitations, many investigators have shifted to NIR wavelength (700 to 900 nm) imaging where photons of light can more easily penetrate tissue, allowing detection of deeper structures such as collecting vessels or lymph nodes located under the skin. An early focus of this work was centered on the use of NIR quantum dots, which are extremely bright nanoparticles containing a core of heavy metals, for SLN detection [158]. They can be easily tuned to a wide variety of wavelengths, a fact that was exploited in a study by Kobayashi et al., to simultaneously map five lymph node basins in a single mouse [159]. Despite this great promise, toxicity concerns have limited the potential of quantum dots, with one study demonstrating particles remaining in reticular organs of mice even two years after intravenous injection [160].

Similar to clinical NIR lymphography, studies using custom imaging devices in both swine and murine models have demonstrated that collecting lymphatic vessels can be visualized in a dynamic manner after intradermal ICG injection [161–163]. Although it is inexpensive and has an excellent safety profile, ICG has many drawbacks in its native form for lymphatic imaging. It is a weak fluorescent dye with poor

Please cite this article as: A.K. Polomska and S.T. Proulx, Imaging technology of the lymphatic system, Adv. Drug Deliv. Rev., https://doi.org/10.1016/j.addr.2020.08.013

stability that exhibits self-quenching in solution. Furthermore, both lymphatic specificity and the brightness of the dye are dependent on protein binding in the interstitium, which may not always occur sufficiently depending on the dose administered and the state of the tissue [90,164]. Our group has formulated a more stable formulation of ICG by encapsulating it in the lipid bilayer of pegylated liposomes of approximately 60 nm diameter [100]. Upon intradermal injection, the increased brightness of this formulation over native dye and the specificity for the lymphatic system allowed detection of lymph nodes up to 1 cm deep in mice with a commercially available whole animal imaging system. ICG has also been encapsulated in micelles [91], embedded in nanogels [165], complexed to polymers [102], lipid nanoparticles [99] or pre-mixed with albumin [166–168] for lymphatic imaging.

New fluorescent tracers for preclinical lymphatic imaging based on conjugates of the bright NIR dye, IRDye, and PEG polymers have been introduced [90,169]. We found that conjugates composed of > 10 kDa PEG molecules were exclusively drained by the lymphatic vessels after injection into skin. Unlike dextrans or quantum dots, uptake by phagocytes with subsequent retention in the draining lymph node was not detectable [3]. These particles also appear to be biologically inert with little adhesion to constituents of the extracellular matrix or lymphatic endothelium. Weiler and Dixon have found that use of PEG-dye conjugates prevented the detrimental effects on lymphatic contractility and expansion of the lymph node that occurs for many days after an injection of ICG into the rat tail [167]. In both solution and in vivo, PEG-dye conjugates exhibit excellent stability with clearance in intact form through the kidney from the blood circulation [90].

Microscopic systems have been customized for sensitive imaging in the NIR spectrum. Adaptation of commercially available stereo or zoom epifluorescence microscope setups with the addition of appropriate filters, light sources and NIR-sensitive cameras, has enabled noninvasive in vivo image acquisition of lymphatic vessels with high spatial and temporal resolution (Fig. 2C) [90,166]. These methods have been employed to visualize alterations in lymphatic function and flow rerouting in animal models of cancer and lymphedema [90,170–172]. The techniques have also gained utility to evaluate lymphatic function in transgenic models of genes responsible for the growth and/or maintenance of lymphatic vessels [173,174]. Similarly, utilization of tracer injections into lymphatic transgenic reporter mice enables a combined functional and anatomical imaging approach that has allowed mapping of lymphatic drainage from the skin, the peritoneal cavity and the central nervous system [131,132,175,176]. The non-invasive nature of NIR imaging and the favorable characteristics of the lymphatic-specific tracers have stimulated the development of several quantitative measures of the lymphatic system in preclinical models, as outlined later in this review.

3.2.4. Photoacoustic imaging

Photoacoustic imaging, also known as optoacoustic imaging, is a hybrid imaging technique that combines optical absorption and ultrasound detection. The tissue of interest is illuminated with a short pulsed, non-ionizing light. After the light is absorbed by the tissue components, heat is generated that leads to thermoelastic expansion and thus ultrasonic emission. The generated ultrasound waves are measured with transducers to generate an image. Therefore, this technique is often referred to as "light in, sound out" [177]. Since ultrasound waves can be detected with high resolution, at greater depths and with less scattering than optical imaging, this imaging modality has tremendous promise for the imaging of lymphatic vessels and lymph nodes in both animal models and humans. However, unlike blood vessels, which can be detected with photoacoustic detectors based upon endogenous signals such as hemoglobin, lymphatic vessels still require exogenous tracers for detection. Photoacoustic imaging is highly scaleable, with very high spatial resolution, albeit at low depth penetration, using photoacoustic microscopy or with a higher depth penetration up to several cm but lower resolution using photoacoustic tomography [177–179].

Initial studies using this imaging modality to visualize the lymphatic system focused on the detection of lymph nodes, mostly for SLN mapping applications [180,181]. For example, Erpelding et al., utilized intradermal injections of methylene blue dye to visualize axillary lymph nodes in rats. The authors were able to prove that signals within lymph nodes that were located 2.5 cm below the imaging probe could be detected by adding chicken breast samples on top of the rat skin surface [182]. Further development of this technology allowed visualization of collecting lymphatic vessels afferent to the axillary lymph node of rats after injections of nanoparticles such as gold nanostars [183].

The potential of this technique for lymphangiography was pushed further with a photoacoustic microscopy approach to image lymphatic vessels in the tail and ear skin of mice after Evans blue dye injections [184]. Using multispectral imaging, the authors were able to simultaneously visualize the blood vessels using the endogenous hemoglobin signals (Fig. 2D). In multispectral imaging, a series of images is recorded at different wavelengths. Based on the knowledge of absorption spectra of the molecules of interest (e.g. ICG) and the background molecules, their distribution can be determined using spectral unmixing algorithms. However, the exact quantification of the absorber concentration at depth requires correction due to the fact that the attenuation of the light varies with the wavelength [185]. Another group utilized a commercially available photoacoustic imaging system to visualize the pumping of collecting lymphatic vessels at 3 to 5 mm deep in the hind limb of mice [186]. The authors assessed the potential of several different dyes, including Evans blue and ICG, for this assay and detected contraction rates similar to those assessed by NIR imaging in isoflurane-anesthetized mice [187,188].

3.2.5. Optical coherence tomography

Optical coherence tomography is a technique that allows label-free 3D reconstruction of the optical scattering within tissues. Lymphatic vessels have been shown to be "visible" with this technique through negative contrast from high-scattering surrounding tissue and can be further differentiated from blood vessels due to the presence of few intraluminal cells (Fig. 2E) [189–191]. The technique allows rapid volumetric scanning, enabling dynamic quantifications of collecting lymphatic function as outlined below. However, similar to other fluorescence methods, the imaging is limited by depth, in this case to structures less than 2 mm below the tissue surface. With a microscopic OCT approach, lymphatic vessels have been rendered within the cornea of mice that have been treated with sutures to induce inflammatory lymphangiogenesis [192]. Conjunctival lymphatic vessels have been visualized ex vivo in porcine eyes by another group [193]. Further studies are necessary to evaluate the potential of this technique for imaging of ocular lymphatic vessels in the clinic.

4. Pre-clinical and clinical quantitative imaging assessments of lymphatic function

The advancements that have been made in tracer design and imaging technology detailed in the previous sections of this review have enabled several different methods for quantifying the function of the lymphatic system to be developed. These quantitative measures have improved preclinical studies by allowing unbiased assessments of interventions aiming to stimulate or diminish lymphatic transport and serve as emerging diagnostic markers for the clinic. We will first describe methods that have focused on assessing the function of collecting lymphatic vessels and then discuss techniques that can measure lymphatic transport from a tissue of interest.

4.1. Collecting lymphatic vessel contractility

The contractility of collecting lymphatic vessels is traditionally studied in preparations of isolated lymphatic vessels, dissected from such species as sheep, rabbits or rats [194–196]. These methods have recently

Please cite this article as: A.K. Polomska and S.T. Proulx, Imaging technology of the lymphatic system, Adv. Drug Deliv. Rev., https://doi.org/10.1016/j.addr.2020.08.013

been adapted to mice, allowing investigation of a wide variety of transgenic mouse models [197,198]. In these setups, parameters such as infusion pressure and temperature can be easily controlled and modulated. Thus, much has been learned from these studies regarding the physiology of collecting lymphatic vessels and the factors that control their contractility and valve function. However, the limitations due to the ex vivo nature of these studies have led to a significant push to develop in vivo imaging methods in which vessels can be studied under more physiological conditions, as well as in preclinical models of human disease.

The group of Timothy Padera has developed an intravital microscopy technique for the imaging of popliteal collecting lymphatic vessels after FITC-dextran injection into the footpad of mice [199]. Dynamic video acquisition of the contractility of the lymphatic vessels in mice was possible for the first time, however, a surgical dissection of the skin overlaying the vessels and a positioning of the mouse in an upright position were necessary in order to allow imaging on an inverted microscope. Nonetheless, this method has shed light on the effects of different cellular sources of nitric oxide on lymphatic contractility.

Early reports describing noninvasive NIRF techniques to visualize collecting lymphatic vessels have reported quantifications of the frequency or velocity of "ICG packet transport" or "pulsations" [90,162,187]. It was unclear exactly what these measurements represented in the context of the contractility of the collecting vessels or the overall efficiency of lymph transport. It was also evident that measurements of frequency alone would only tell one part of the story, as contraction strength or amplitude was not assessed. Indeed, a recent study has shown that measurements of frequency had no direct correlation with estimates of overall lymph transport [200]. The wide variety of frequencies of these events reported in the literature was another source of confusion [188].

Using an exteriorized preparation of the flank collecting lymphatic vessel in Prox1-GFP mice, we have shown that measurements of vessel diameter are directly correlated with the intensity of fluorescence that is measured using a region of interest covering the vessel (Fig. 3A) [201]. This has since been confirmed by another study in rats from the group of Brandon Dixon [200]. Thus, these studies have demonstrated that measurements of fluorescence signal intensity dynamics, as may be recorded in a noninvasive fashion, can provide information on contraction strength as well as frequency. Our group and others have developed analysis algorithms for the evaluation of contraction frequency and amplitude based on NIR fluorescence imaging (Fig. 3B) that have

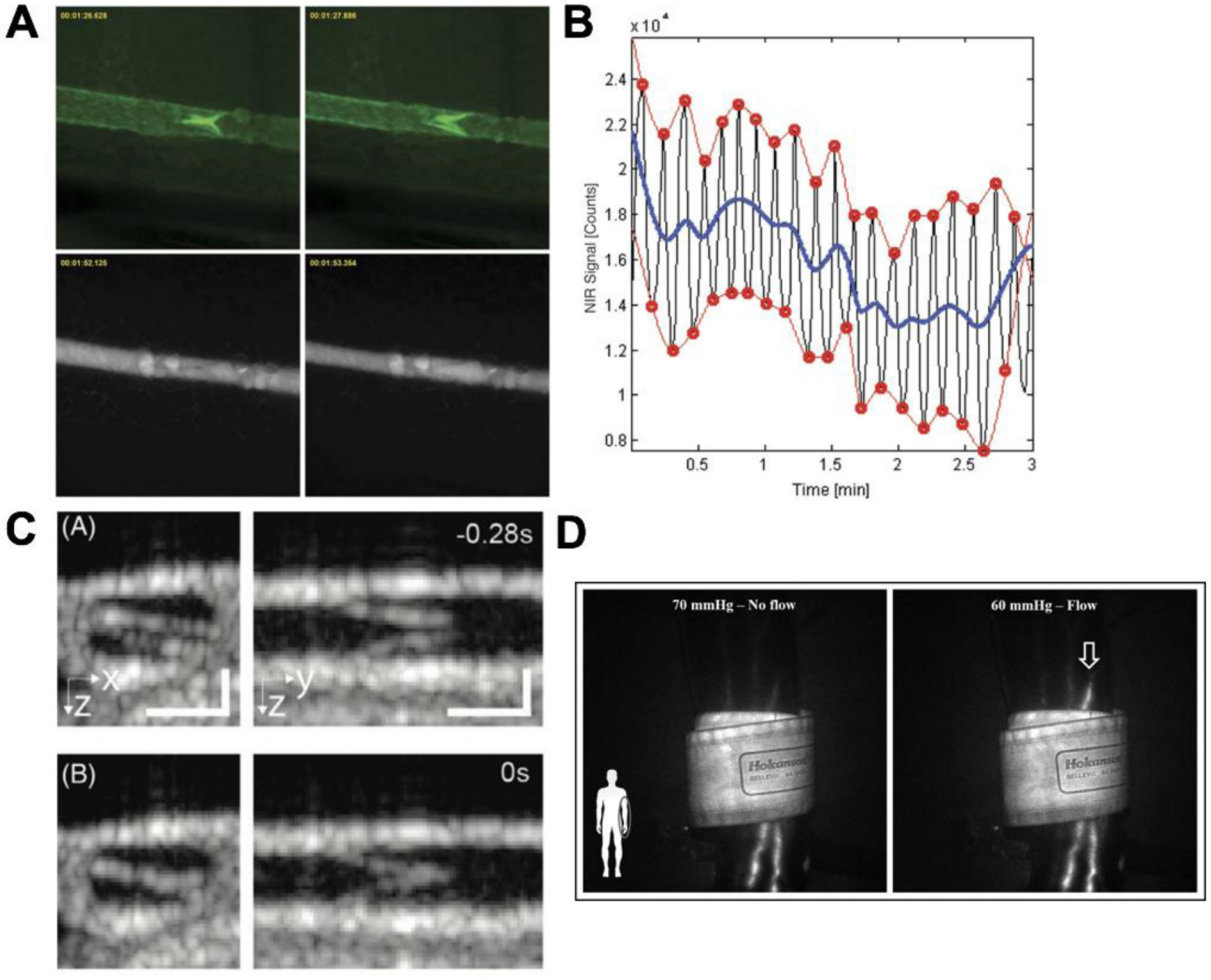

Fig. 3. Imaging methods allowing quantification of collecting lymphatic vessel function. (A) Fluorescence microscopy visualization of a contractile collecting lymphatic vessel and valve in a Prox1-GFP transgenic reporter mouse flank after infusion of PEGylated tracer into the inguinal lymph node. Images of endogenous GFP signal (upper) and NIR tracer (below) at different stages of the contraction cycle. (B) Example semi-automated analysis plot with peak detection (red circles) and mean signal intensity (blue line) for quantification of collecting lymphatic vessel contraction frequency and amplitude from NIR imaging. Reproduced from [201]. (C) Doppler OCT cross-sectional images perpendicular to (left) and along (right) a collecting lymphatic vessel and valve in the mouse hind limb at different stages of the contraction cycle. Reproduced with permission from [206] (D) Illustration of pumping pressure measurement in the upper arm using NIR lymphography in humans. Lymphatic pumping pressure is defined as the cuff pressure when the ICG dye exceeded the upper border of the cuff (arrow). Reproduced with permission from [50]. (For interpretation of the references to colour in this figure legend, the reader is referred to the web version of this article.)

Please cite this article as: A.K. Polomska and S.T. Proulx, Imaging technology of the lymphatic system, Adv. Drug Deliv. Rev., https://doi.org/10.1016/j.addr.2020.08.013

allowed a semi-automated assessment of potential factors influencing collecting lymphatic vessel function [200–202]. These in vivo analysis techniques can thus complement the findings from ex vivo studies of collecting lymphatics.

Direct measurements of the pumping frequency, amplitude and pumping velocity using NIR fluorescence imaging are also possible in humans [44,48–51]. According to recent publications from a clinical group in Denmark, these parameters have low intra-individual and intra-observer variability in legs and arms that suggest that they may be used to evaluate the function of the lymphatic vessels in health and disease [50,51].

We have found that one source of disparity in the observed frequencies from different research groups were the effects of different anesthesia regimens on contractility [188]. For example, isoflurane has been shown to decrease lymphatic contraction rates in a dose dependent fashion [203]. Other factors such as animal positioning and injection volume also appear to play significant roles [204]. Indeed, the requirement for an injected tracer to perfuse the lymphatic vessel is a severe limitation of these quantitative in vivo methods, as there is known to be a direct effect of intraluminal pressure on collecting lymphatic vessel contractility [197]. This can be easily observed after an external compression (i.e. massage) of the injection site, which loads more tracer into the downstream lymphatic vessels and has immediate effects on the contractility rates [90].

To address this limitation, Blatter and colleagues have explored the capability of a tracer-free Doppler OCT (DOCT) technique for the assessment of lymphatic flow [205,206]. DOCT systems are able to measure the motion of scattering particles in the tissue. Using B-mode Doppler methods, acquisition rates of 50 Hz can be achieved. By monitoring the movement of particles within the lymphatic vessels or the motion of the surrounding tissue the authors are able to estimate parameters of lymphatic contractility. Visualization of the lymphatic valve function is also possible with these techniques (Fig. 3C). However, one existing limitation with this technique is that the skin above the collecting lymphatic vessels needs to be surgically dissected due to its high amount of optical scattering.

4.2. Lymphatic pumping pressure

A clever quantitative approach for measuring lymphatic function estimates the pumping pressure of the collecting lymphatic vessels. This technique was first developed in the clinic by combining lymphoscintigraphic imaging with an inflatable pressure cuff [207]. Pumping pressure has been proposed to be a relevant parameter that correlates with the intrinsic active contractile function of the lymphatic collectors and extrinsic forces such as muscular activity that drive lymph propulsion against an increasing hydrostatic pressure gradient. In this method, an inflatable congestion pressure cuff is applied on the limb and an interstitial lymphatic tracer is injected distal to the cuff. While the pressure of the cuff is gradually reduced, the whole limb is dynamically imaged until the tracer flow is restored. The effective pumping pressure of the lymphatic vessels is the pressure reading at which the vessels are capable of transporting the tracer through the cuff. Using this technique in combination with lymphoscintigraphy, it was demonstrated that women who developed lymphedema after breast-cancer related lymphadenectomy 2 years post-surgery had a higher pre-operative pumping pressure compared to those that did not develop the disease [14]. This surprising result was determined from a relatively small group of patients and requires further confirmation. Pumping pressure has also been determined in human upper and lower limbs using the cuff method combined with ICG imaging (Fig. 3D) [50,51,208–210].

Nelson and colleagues have established these techniques for the estimation of lymphatic pumping pressure in collecting lymphatic vessels of the rat [172]. The system was validated with the application of a nitric oxide donor cream that has been shown to inhibit lymphatic contractility. In a further study, the technique was used to demonstrate that the effective pumping pressure generated in the rat tail is dependent on the location of the pressure cuff. When the cuff was placed near the base of the tail the pressure generated was significantly higher than when the cuff was located more distally. The authors attributed this difference to the number of lymphangions available to generate the contractile forces [211]. The technique was also recently applied by the same group to assess the functionality of collecting lymphatic vessels in a lymphatic injury model in the hind limbs of sheep [172].

4.3. Lymphatic clearance

Perhaps the simplest method to quantify lymphatic function is to monitor the disappearance (clearance) of injected tracers at the site of injection. A clinical scintigraphic method that can track lymphatic removal of an interstitial depot of radiolabeled tracer has been established for assessment of the lymphatic function in patients with lymphedema [27]. One obvious limitation of a scintigraphic-based clearance method is the need to take into consideration the radioactive half-life of the tracer. Using fluorescence imaging, preclinical techniques for measuring lymphatic clearance have been established using human albumin labeled with fluorescent dye [212], PEGylated NIR dyes [213] or ICG non-covalently bound to non-toxic polymer [102] or encapsulated in micelles [91]. In each case, lymphatic function can be modeled as a one-phase exponential decay over time (Fig. 4A). Advantages of this technique include the need for only minute amounts of tracer, the ability to measure rapidly and the requirement for relatively few measurements to fit to the decay model. This means that measurements can be performed in animals that are only shortly anesthetized or manually restrained, thus allowing the clearance of the tracer to occur under normal physiological conditions between timepoints. Using this technique, we have compared the effect of aging on lymphatic clearance from the mouse ear skin and have found a significant decrease in the clearance rate in aged versus young animals [213]. Another group has shown that clearance can be monitored with NIR imaging from the knee joints in rats after intraarticular injection of PEGylated tracers [214]. Lymphatic clearance assessments have also been recently established using photoacoustic imaging. Yücel et al., have developed a technique in which the clearance of a NIR quencher dye, QC-1, bound to bovine serum albumin was tracked after injection into the anterior chamber of the eye in mice [215].

4.4. Tracer transport to lymph nodes and/or blood

In the past, in vivo measurements of lymph flow in animal models from a specific anatomical site required surgical procedures such as cannulation of collecting lymph vessels for tracer recovery. The complicated anatomy of the lymphatic system, with multiple collecting vessels draining each organ and inconsistent routing of these vessels between individual subjects was a severe limitation of such studies. In rodents, such methods are technically demanding due to the small size of the collectors and have thus been restricted to larger lymphatic trunks, such as the thoracic duct [216]. Imaging approaches have thus largely replaced these methods by using non-invasive measures of tracer flow through draining lymph nodes or to the systemic blood circulation.

Several imaging modalities have the sensitivity and resolution capable of detecting signal intensity dynamics of lymphatic tracers within lymph nodes. As mentioned previously, such assessments have been made with PET/CT, MRI and fluorescence imaging techniques [100,131,137]. Depending on the tracer, lymph node signals will either increase steadily over time (as a measure of tracer retention) or will initially increase and then decrease (as a measure of lymph flow through the node) [3]. The first approach would be more desirable for the optimization of drug delivery or diagnostic techniques targeting the lymph node, while the second approach is more suited for assessment of lymphatic function.

Please cite this article as: A.K. Polomska and S.T. Proulx, Imaging technology of the lymphatic system, Adv. Drug Deliv. Rev., https://doi.org/10.1016/j.addr.2020.08.013

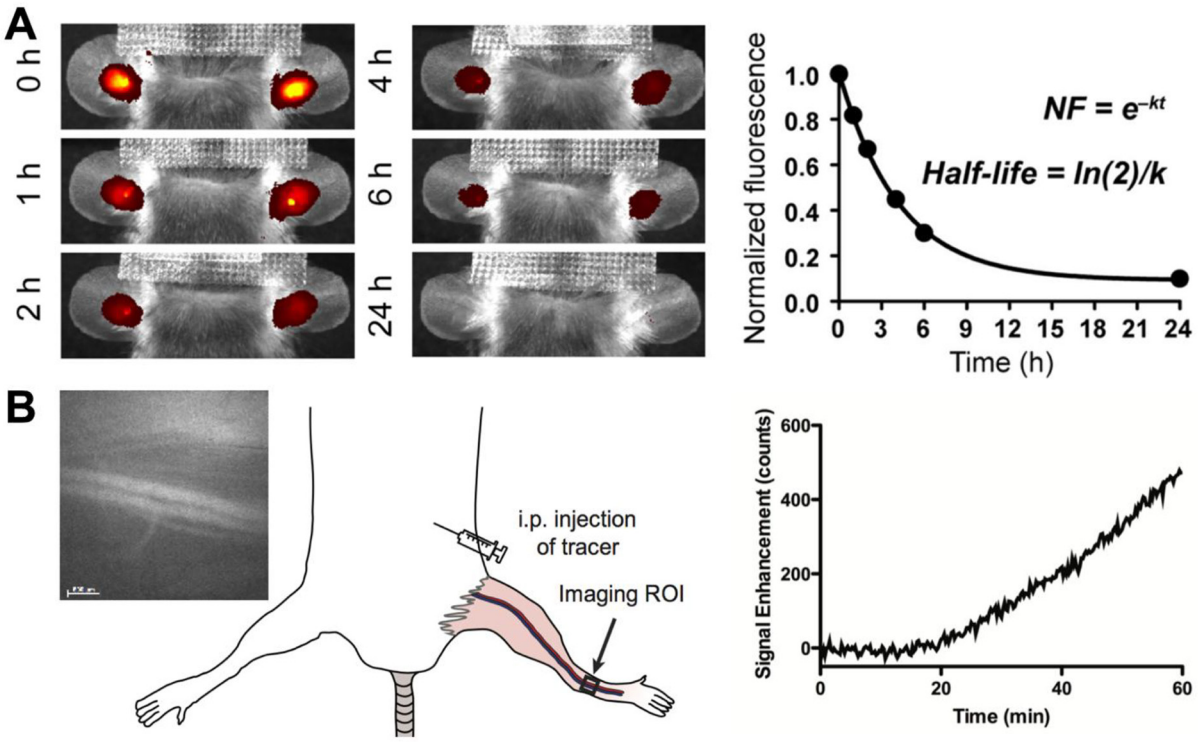

Fig. 4. NIR fluorescence imaging methods allowing quantification of lymphatic tracer clearance and tracer transport to blood in mice. (A) Lymphatic clearance assay of PEGylated tracers in mouse ear skin. Images are acquired at several time points after injection (left panels) and the loss of normalized fluorescence (NF) intensity exhibits a one-phase exponential decay over time (right panel). Equations for the lymphatic clearance rate k and the half-life of clearance can be solved as measures of lymphatic function. Modified with permission from [213]. (B) Lymphatic transport to blood assay after intraperitoneal (i.p.) injection of PEGylated 40 kDa fluorescent tracers. After tracer injection, images are acquired at a saphenous vein region of interest (ROI) with a fluorescence stereomicroscope (example image in left panel) and plotted over time to indicate the transport of the tracer to the systemic blood through the lymphatic system (right panel). Modified from [175].

Our group has developed a method to quantify the dynamics of NIR tracers in the draining lymph node after injection into the skin of mice [100]. As an intradermal administration leads to almost immediate filling of the lymph node after the injection, modeling of the clearance of the inert tracer over time as a one-phase exponential decay gives a rudimentary measure of the lymph flow through the node. We have used this technique in conjunction with ICG liposomes to demonstrate the blockage of flow through a lymph node that is bearing metastatic tumor cells and a reduction of lymphatic clearance from chronically-inflamed skin [100,217]. However, methods quantifying tracer dynamics in draining lymph nodes are highly dependent on the accuracy of the injection and require anesthesia for the imaging of the lymph nodes in consistent position over time. As discussed above, such quantifications are also complicated by the fact that many organs have multiple drainage basins with several potential lymph nodes draining the injected tracers.

To address some of these limitations, an alternative approach of detecting the accumulation of a lymphatic-specific tracer in the systemic blood has been developed [175,218,219]. As all lymphatic routes eventually lead to the bloodstream, this approach simplifies the quantification of tracer transport from a specific organ. Previous approaches required cannulation, however, using PEGylated fluorescent tracers of 40 kDa size, we have found that non-invasive measures of lymphatic transport to blood can be made with high sensitivity in mice by NIR monitoring of the signal dynamics in a large superficial blood vessel [175]. This method allows deeper organs or anatomical cavities to be assessed, as demonstrated for the peritoneal cavity (Fig. 4B). Using these measures, we have demonstrated the necessity for tissue motion for tracers to access the initial lymphatic vessels of the skin. After subcutaneous injection into anesthetized mice, there was no detectable transport through the lymphatic system to the systemic circulation. If a periodic massage protocol of the injected skin was employed, the transport to the blood in the anesthetized mice was similar to levels seen in awake animals. This method has also been further utilized to reveal that inert tracers injected into the CSF of mice appear to drain exclusively through routes leading to lymphatic vessels, instead of directly to veins as commonly thought [132,220]. These techniques have also revealed that CSF outflow to lymphatics is substantially increased in awake conditions and is reduced in aged mice. Limitations of this technique include the need for large amounts of injected tracer and the requirement of the tracer to have a long plasma circulation for sensitive dynamic assessments in the systemic blood.

5. Emerging imaging techniques for the clinic

In the final section of this review, we will describe how new imaging technology is being translated to the clinic for visualization and quantification of the lymphatic system. As we have detailed, many pre-clinical studies have focused on the development and application of novel safe, stable, bright and highly lymphatic-specific tracers. Despite excellent performance in animal studies of some of these tracers, very few are being translated to the clinics, likely due to the low potential of patent protection, high costs of clinical testing and minimal interest of pharmaceutical companies. Thus, most recent clinical efforts have been on the development of systems that can use existing tracers, such as ICG, or can provide information in a tracer-free manner, such as ultra high-frequency ultrasound.

Among new imaging modalities, photoacoustic imaging is a most promising technique as it allows for real-time imaging of the lymphatic structures at high depths (~2.5 cm) and excellent spatial resolution (~160 μm) using safe and well-established optical tracers, such as ICG. While the low quantum yield of ICG makes it not an ideal tracer for

Please cite this article as: A.K. Polomska and S.T. Proulx, Imaging technology of the lymphatic system, Adv. Drug Deliv. Rev., https://doi.org/10.1016/j.addr.2020.08.013

NIR fluorescence imaging, this property represents an advantage in the context of photoacoustic imaging, because of an improved conversion of absorbed light energy to heat. Photoacoustic visualization systems for clinical applications are not commercially available yet. However, prototype devices (such as PAI-05 and AcoustiX) have been used for simultaneous imaging of the lymphatic and blood vessels in published clinical studies [221–223].

Using the PAI-05 system, strikingly sharp images of the lymphatic and blood vasculature network in a large field of view in the limbs of healthy volunteers and lymphedema patients have been recently obtained, on which superficial lymphatic vasculature with dermal backflow of ICG, as well as the deeper collecting vessels, could be visualized (Fig. 5A) [223]. On the other hand, the AcoustiX system was able to visualize the lymphatics along with the blood vessels in real time in a smaller field of view (50 × 7 mm) up to 2.6 cm below the skin; however, the overall OA image quality is lower compared to that obtained using PAI-05 [222]. A disadvantage of both devices lies in their large size and the fact that the limb has to be immersed in a water bath for the measurement. In contrast, a multispectral optoacoustic imaging tomography (MSOT) system (MSOT Acuity Echo) can be operated in a hand-held 3D mode and only ultrasound gel is necessary for the imaging, which enables performance of this procedure at the bedside. This prototype system allowing both OA and US imaging modes is now available for clinical studies, while its predecessor model (MSOT Acuity - without the US imaging capability) has been recently CE-marked [107]. In a small study with 11 lymphedema patients, MSOT Acuity Echo was used to visualize lymphatic vessels in the limbs in regions that were concealed by dermal backflow in ICG lymphography. The capability of real-time 3D simultaneous imaging of blood and lymphatic vessels with good spatiotemporal resolution makes MSOT especially valuable for choosing the appropriate sites for the LVA [224]. Photoacoustic imaging has also been tested in humans in the context of SLNs and detecting metastatic burden in melanoma patients [225,226]. In sum, further development is still required for clinical instrumentation, imaging probes and protocols for photoacoustic imaging in the context of the lymphatic system. However, the recent increase

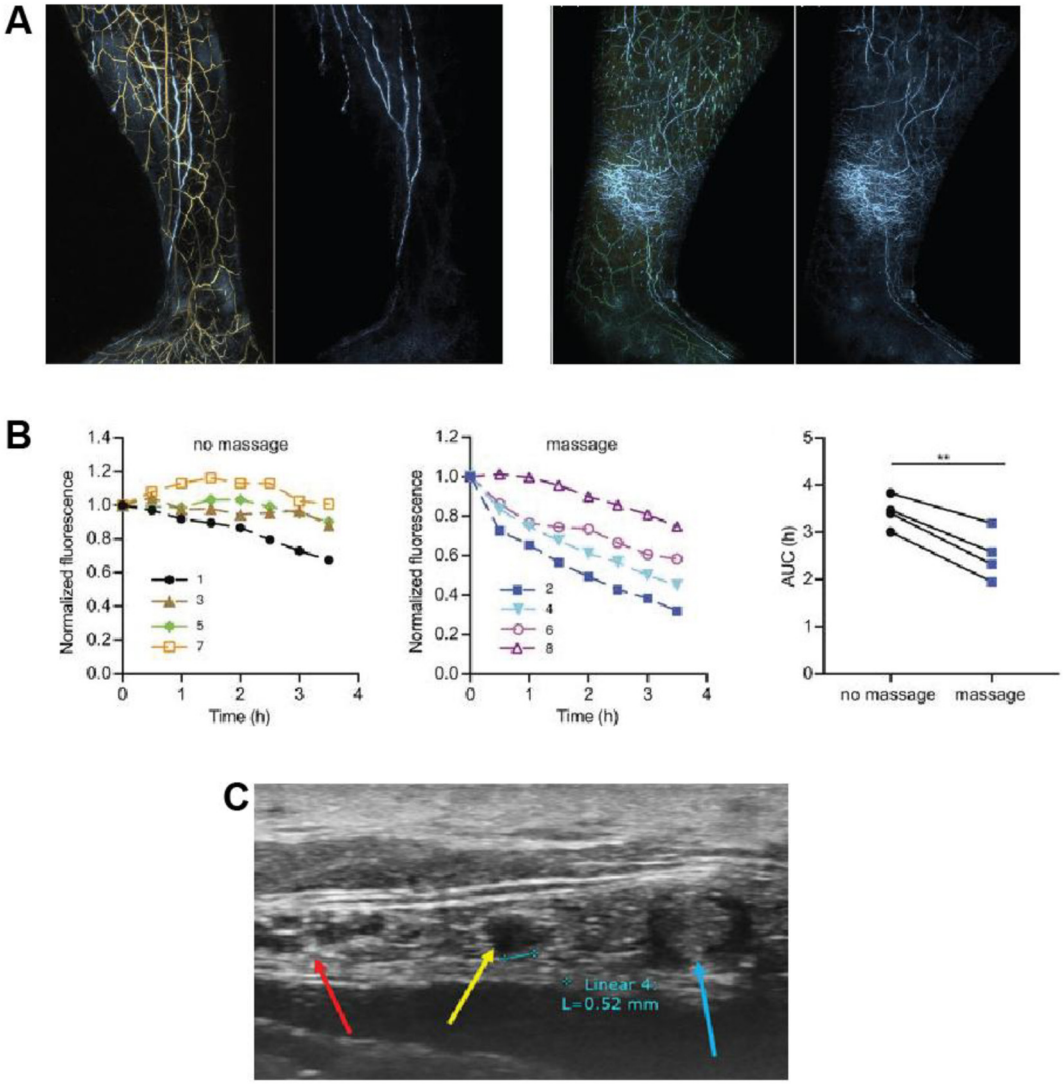

Fig. 5. Emerging clinical imaging techniques. (A) Optoacoustic imaging. Medial side view of the photoacoustic lymphangiography of the healthy lower leg (first two images from the left) and in legs with lymphedema (third and fourth images). Images showing both blood and lymphatic vessels (first and third) and only lymphatics (second and fourth). Dermal backflow and fine network of dermal lymphatic vessels are observed in the extremity with lymphedema. Reprinted with permission [223]. (B) Quantitative assessment of lymphatic function in pigs with ICG-Kolliphor HS15 and hand-held device. Normalized signal disappearance at the massaged and not massaged injection sites and signal quantification with the AUC. The fluorescence signal was measured using a custom hand-held device without imaging capability [91]. (C) Ultra high frequency ultrasound. Imaging in the posterior aspect of the lower leg. Lymphatic vessels (yellow arrows), small saphenous vein (blue arrow) and sural nerve (red arrow) [227]. (For interpretation of the references to colour in this figure legend, the reader is referred to the web version of this article.)

Please cite this article as: A.K. Polomska and S.T. Proulx, Imaging technology of the lymphatic system, Adv. Drug Deliv. Rev., https://doi.org/10.1016/j.addr.2020.08.013

of pre-clinical and clinical studies in this field suggests that this technique is likely to be embraced for routine application in patients.

In a recent study from our group, we investigated in pigs a clinically-relevant technique for quantification of the lymphatic clearance based on measuring the disappearance of the tracer at the injection site after intradermal administration. In this method, ICG was encapsulated in micelles of polyoxyl 15 hydroxystearate (Kolliphor HS15) that prevented self-quenching, increased the quantum yield and improved the stability of the dye in solution. The ICG-Kolliphor HS15 solution was injected using MicronJet600™ microneedles (Nanopass Ltd) that allowed for precise and pain-free intradermal administration. We measured the fluorescence signal over time using a custom-made hand-held device that allows simple NIR-fluorescence signal quantification without the need for imaging capability. In particular, in this study, we demonstrated differences in lymphatic clearance in different parts of the pig abdomen and upon application of manual stimulation (massage) (Fig. 5B). The clearance was quantified by calculating the area under the normalized clearance curves (AUCs) [91]. We are currently investigating the feasibility of this technique to quantify lymphatic clearance in patients with established unilateral extremity lymphedema.

Ultra-high frequency ultrasound imaging is characterized by the improved resolution and quality of the image compared to conventional ultrasound. Recently, ultra-high frequency ultrasound, operating at 70 kHZ was used to visualize subcutaneous lymphatic vessels of a diameter smaller than 30 μm, as well as of the lymphatic flow and lymphatic valves in some vessels (Fig. 5C) [227,228]. On the US images, the lymphatic vessels can be identified as intermittent homogenous, hypoechoic and specular misshapen structures [227–232]. In contrast to blood vessels, lymphatic vessels do not collapse upon applying pressure with the transducer head [227,232,233]. US can be used for visualization of the lymphatic vessels for LVA surgery. The major advantage of using US over ICG imaging before LVA as well as intraoperatively is the possibility to visualize the lymphatic and blood vessels in a region where they are concealed by a dermal backflow pattern of ICG [227,228].

In conclusion, the lymphatic imaging modalities described in this review can allow for qualitative visualization and quantitative assessment of the lymphatic system. While most of the techniques require interstitial injection of the tracer to provide contrast between the tissue and lymphatic structures, some emerging techniques are allowing visualization of lymphatics in a tracer-free manner. In clinical settings, lymphatic imaging is predominantly being performed with conventional tracers that have been approved since several years or even decades. Further development is focused mainly on improvement of measurement protocols and defining new quantitative parameters. Although the techniques and tracers for visualization of the lymphatic system are less developed than for the other anatomical structures, with the recent increased attention to lymphatic system function and development, we anticipate continued improvement in lymphatic imaging technology in the coming years.

Funding

Imaging-related research by the authors has been supported by the Skintegrity consortium, a University Medicine Zurich flagship project.

Acknowledgements

The authors would like to thank Prof. Michael Detmar for his continued guidance and support.

References

[1] J.W. Breslin, Y. Yang, J.P. Scallan, R.S. Sweat, S.P. Adderley, W.L. Murfee, Lymphatic vessel network structure and physiology, Compr. Physiol. 9 (2019) 207–299.
[2] E.M. Sevick-Muraca, S. Kwon, J.C. Rasmussen, Emerging lymphatic imaging technologies for mouse and man, J. Clin. Invest. 124 (2014) 905–914.
[3] S.T. Proulx, P. Luciani, L.C. Dieterich, S. Karaman, J.C. Leroux, M. Detmar, Expansion of the lymphatic vasculature in cancer and inflammation: new opportunities for in vivo imaging and drug delivery, J. Control. Release. 172 (2013) 550–557.
[4] L.L. Munn, T.P. Padera, Imaging the lymphatic system, Microvasc. Res. 96 (2014) 55–63.
[5] J.R. Levick, C.C. Michel, Microvascular fluid exchange and the revised Starling principle, Cardiovasc. Res. 87 (2010) 198–210, https://doi.org/10.1093/cvr/cvq062.
[6] P.S. Mortimer, S.G. Rockson, New developments in clinical aspects of lymphatic disease, J. Clin. Invest. 124 (2014) 915–921.
[7] C.C. Pieper, S. Hur, C.M. Sommer, G. Nadolski, G. Maleux, J. Kim, M. Itkin, Back to the future: Lipiodol in lymphography-from diagnostics to theranostics, Investig. Radiol. 54 (2019) 600–615.
[8] D. Pavlista, O. Eliska, Analysis of direct oil contrast lymphography of upper limb lymphatics traversing the axilla – a lesson from the past – contribution to the concept of axillary reverse mapping, EJSO 38 (2012) 390–394.
[9] R. Lambertz, D.H. Chang, T. Hickethier, M. Bagheri, J.M. Leers, C.J. Bruns, W. Schroder, Ultrasound-guided lymphangiography and interventional embolization of chylous leaks following esophagectomy, Innov. Surg. Sci. 4 (2019) 85–90.
[10] M. Toliyat, K. Singh, R.C. Sibley, M. Chamarthy, S.P. Kalva, A.K. Pillai, Interventional radiology in the management of thoracic duct injuries: anatomy, techniques and results, Clin. Imaging 42 (2017) 183–192.
[11] O.W. Johnson, J.F. Chick, N.R. Chauhan, A.H. Fairchild, C.M. Fan, M.S. Stecker, T.P. Killoran, A. Suzuki-Han, The thoracic duct: clinical importance, anatomic variation, imaging, and embolization, Eur. Radiol. 26 (2016) 2482–2493.
[12] T. Gruber-Rouh, N.N.N. Naguib, T. Lehnert, M. Harth, A. Thalhammer, M. Beeres, I. Tsaur, R. Hammersting, J.L. Wichmann, T.J. Vogl, V. Jacobi, Direct lymphangiography as treatment option of lymphatic leakage: indications, outcomes and role in patient's management, Eur. J. Radiol. 83 (2014) 2167–2171.
[13] F. Celebioglu, L. Perbeck, J. Frisell, E. Grondal, L. Svensson, R. Danielsson, Lymph drainage studied by lymphoscintigraphy in the arms after sentinel node biopsy compared with axillary lymph node dissection following conservative breast cancer surgery, Acta Radiol. 48 (2007) 488–495.
[14] V. Cintolesi, A.W. Stanton, S.K. Bains, E. Cousins, A.M. Peters, A.D. Purushotham, J.R. Levick, P.S. Mortimer, Constitutively enhanced lymphatic pumping in the upper limbs of women who later develop breast cancer-related lymphedema, Lymphat. Res. Biol. 14 (2016) 50–61.
[15] S. Yang, W. Bao, X. Bai, C. Gao, B. Zhang, Z. Jiang, (99m)Tc-labeled sodium phytate and stannous chloride injection accurately detects sentinel lymph node in axillary of early stage breast cancer: a randomized, controlled study, Onco. Targets Ther. 11 (2018) 1891–1898.
[16] M. Pappalardo, C. Lin, O.A. Ho, C.F. Kuo, C.Y. Lin, M.H. Cheng, Staging and clinical correlations of lymphoscintigraphy for unilateral gynecological cancer-related lymphedema, J. Surg. Oncol. 121 (2019) 422–434.
[17] S. O'Mahony, C.K. Solanki, R.W. Barber, P.S. Mortimer, A.D. Purushotham, A.M. Peters, Imaging of lymphatic vessels in breast cancer-related lymphedema: intradermal versus subcutaneous injection of 99mTc-immunoglobulin, AJR Am. J. Roentgenol. 186 (2006) 1349–1355.
[18] L. Wei, F. Chen, X. Zhang, D. Li, Z. Yao, L. Deng, G. Xiao, (99m)Tc-dextran lymphoscintigraphy can detect sentinel lymph node in breast cancer patients, Exp. Ther. Med. 9 (2015) 112–116.
[19] J.T. Unkart, A. Hosseini, A.M. Wallace, Tc-99m tilmanocept versus Tc-99m sulfur colloid in breast cancer sentinel lymph node identification: results from a randomized, blinded clinical trial, J. Surg. Oncol. 116 (2017) 819–823.
[20] D.S. Surasi, J. O'Malley, P. Bhambhvani, 99mTc-Tilmanocept: a novel molecular agent for lymphatic mapping and sentinel lymph node localization, J. Nucl. Med. Technol. 43 (2015) 87–91.
[21] B.L. Murphy, A.R. Woodwick, K.M. Murphy, K.J. Chandler, G.B. Johnson, C.H. Hunt, P. Peller, J.W. Jakub, A.C. Homb, (99m)Tc-Tilmanocept versus (99m)Tc-sulfur colloid in lymphoscintigraphy: sentinel lymph node identification and patient-reported pain, J. Nucl. Med. Technol. 47 (2019) 300–304.
[22] A.K. Azad, M.V. Rajaram, W.L. Metz, F.O. Cope, M.S. Blue, D.R. Vera, L.S. Schlesinger, Gamma-Tilmanocept, a new radiopharmaceutical tracer for cancer sentinel lymph nodes, binds to the mannose receptor (CD206), J. Immunol. 195 (2015) 2019–2029.
[23] J.J. Zhang, W.C. Zhang, C.X. An, X.M. Li, L. Ma, Comparative research on (99m)Tc-rituximab and (99m)Tc-sulfur colloid in sentinel lymph node imaging of breast cancer, BMC Cancer 19 (2019) 956.
[24] N. Li, X. Wang, B. Lin, H. Zhu, C. Liu, X. Xu, Y. Zhang, S. Zhai, T. OuYang, J. Li, Z. Yang, Clinical evaluation of 99mTc-rituximab for sentinel lymph node mapping in breast cancer patients, J. Nucl. Med. 57 (2016) 1214–1220.
[25] J. Li, Z. Zhuang, B. Jiang, P. Zhao, C. Lin, Advances and perspectives in nanoprobes for noninvasive lymph node mapping, Nanomedicine (London) 10 (2015) 1019–1036.
[26] M. Pappalardo, M.H. Cheng, Lymphoscintigraphy for the diagnosis of extremity lymphedema: current controversies regarding protocol, interpretation, and clinical application, J. Surg. Oncol. 121 (2020) 37–47.
[27] S. Modi, A.W. Stanton, P.S. Mortimer, J.R. Levick, Clinical assessment of human lymph flow using removal rate constants of interstitial macromolecules: a critical review of lymphoscintigraphy, Lymphat. Res. Biol. 5 (2007) 183–202.
[28] J.N. Yoo, Y.S. Cheong, Y.S. Min, S.W. Lee, H.Y. Park, T.D. Jung, Validity of quantitative lymphoscintigraphy as a lymphedema assessment tool for patients with breast cancer, Ann. Rehabil. Med. 39 (2015) 931–940.
[29] V.M. Moncayo, J.N. Aarsvold, N.P. Alazraki, Lymphoscintigraphy and sentinel nodes, J. Nucl. Med. 56 (2015) 901–907.

Please cite this article as: A.K. Polomska and S.T. Proulx, Imaging technology of the lymphatic system, Adv. Drug Deliv. Rev., https://doi.org/10.1016/j.addr.2020.08.013

[30] D. Hellingman, S. Vidal-Sicart, L.J. de Wit-van der Veen, P. Paredes, R.A.V. Olmos, A new portable hybrid camera for fused optical and scintigraphic imaging: first clinical experiences, Clin. Nucl. Med. 41 (2016) e39–e43.
[31] S. Sajedi, H. Sabet, H.S. Choi, Intraoperative biophotonic imaging systems for image-guided interventions, Nanophotonics 8 (2019) 99–116.
[32] C.K. Kim, K.A. Zukotynski, Desirable properties of radiopharmaceuticals for sentinel node mapping in patients with breast cancer given the paradigm shift in patient management, Clin. Nucl. Med. 42 (2017) 275–279.
[33] T. Iimura, Y. Fukushima, S. Kumita, R. Ogawa, H. Hyakusoku, Estimating lymphodynamic conditions and lymphovenous anastomosis efficacy using (99m)Tc-phytate lymphoscintigraphy with SPECT-CT in patients with lower-limb lymphedema, Plast Reconstr. Surg. Glob. Open 3 (2015), e404.
[34] Y. Naaman, L. Pinkas, S. Roitman, S. Ikher, N. Oustinov, E. Vaisbuch, A. Yachnin, A. Ben-Arie, The added value of SPECT/CT in sentinel lymph nodes mapping for endometrial carcinoma, Ann. Surg. Oncol. 23 (2016) 450–455.
[35] Z.Z. Saad, S. Omorphos, S. Michopoulou, S. Gacinovic, P. Malone, R. Nigam, A. Muneer, J. Bomanji, Investigating the role of SPECT/CT in dynamic sentinel lymph node biopsy for penile cancers, Eur. J. Nucl. Med. Mol. I 44 (2017) 1176–1184.
[36] R.T. Koyyalamudi, M.A. Rossleigh, Lymphoscintigraphic SPECT/CT-contralateral axillary sentinel lymph node drainage in breast bancer, Clin. Nucl. Med. 42 (2017) 121–122.
[37] K. Tew, D. Farlow, SPECT/CT in melanoma lymphoscintigraphy, Clin. Nucl. Med. 41 (2016) 961–963.
[38] M. Simanek, P. Koranda, SPECT/CT imaging in breast cancer - current status and challenges, Biomed. Pap. Med. Fac. Univ. Palacky Olomouc Czech Repub. 160 (2016) 474–483.
[39] A. Bollinger, K. Jager, F. Sgier, J. Seglias, Fluorescence microlymphography, Circulation 64 (1981) 1195–1200.
[40] A. Bollinger, B.R. Amann-Vesti, Fluorescence microlymphography: diagnostic potential in lymphedema and basis for the measurement of lymphatic pressure and flow velocity, Lymphology 40 (2007) 52–62.
[41] H.H. Keo, M. Husmann, E. Groechenig, T. Willenberg, S.B. Gretener, Diagnostic accuracy of fluorescence microlymphography for detecting limb lymphedema, Eur. J. Vasc. Endovasc. Surg. 49 (2015) 474–479.
[42] R.H. Mellor, C.E. Hubert, A.W.B. Stanton, N. Tate, V. Akhras, A. Smith, K.G. Burnand, S. Jeffery, T. Mäkinen, J.R. Levick, P.S. Mortimer, Lymphatic dysfunction, not aplasia, underlies Milroy disease, Microcirculation 17 (2010) 281–296.
[43] S.G. Rockson, A role for near infrared fluorescent imaging in the evaluation of lymphatic function, Lymphat. Res. Biol. 15 (2017) 203.
[44] E.M. Sevick-Muraca, R. Sharma, J.C. Rasmussen, M.V. Marshall, J.A. Wendt, H.Q. Pham, E. Bonefas, J.P. Houston, L. Sampath, K.E. Adams, D.K. Blanchard, R.E. Fisher, S.B. Chiang, R. Elledge, M.E. Mawad, Imaging of lymph flow in breast cancer patients after microdose administration of a near-infrared fluorophore: feasibility study, Radiology 246 (2008) 734–741.
[45] N. Unno, K. Inuzuka, M. Suzuki, N. Yamamoto, D. Sagara, M. Nishiyama, H. Konno, Preliminary experience with a novel fluorescence lymphography using indocyanine green in patients with secondary lymphedema, J. Vasc. Surg. 45 (2007) 1016–1021.
[46] T. Kitai, T. Inomoto, M. Miwa, T. Shikayama, Fluorescence navigation with indocyanine green for detecting sentinel lymph nodes in breast cancer, Breast Cancer 12 (2005) 211–215.
[47] S. Yoneya, T. Saito, Y. Komatsu, I. Koyama, K. Takahashi, J. Duvoll-Young, Binding properties of indocyanine green in human blood, Invest. Ophthalmol. Vis. Sci. 39 (1998) 1286–1290.
[48] M.D. Granoff, A.R. Johnson, B.T. Lee, T.P. Padera, E.M. Bouta, D. Singhal, A novel approach to quantifying lymphatic contractility during indocyanine green lymphangiography, Plast. Reconstr. Surg. 144 (2019) 1197–1201.
[49] A.R. Johnson, M.D. Granoff, B.T. Lee, T.P. Padera, E.M. Bouta, D. Singhal, The impact of taxane-based chemotherapy on the lymphatic system, Ann. Plast. Surg. 82 (2019) S173–S178.
[50] B. Kelly, S. Mohanakumar, N. Telinius, M. Alstrup, V. Hjortdal, Function of upper extremity human lymphatics assessed by near-infrared fluorescence imaging, Lymphat. Res. Biol. 18 (2019) 226–231.
[51] J.H. Groenlund, N. Telinius, S.N. Skov, V. Hjortdal, A validation study of near-infrared fluorescence imaging of lymphatic vessels in humans, Lymphat. Res. Biol. 15 (2017) 227–234.
[52] T. Yamamoto, N. Yamamoto, K. Doi, A. Oshima, H. Yoshimatsu, T. Todokoro, F. Ogata, M. Mihara, M. Narushima, T. Iida, I. Koshima, Indocyanine green-enhanced lymphography for upper extremity lymphedema: a novel severity staging system using dermal backflow patterns, Plast. Reconstr. Surg. 128 (2011) 941–947.
[53] M. Narushima, T. Yamamoto, F. Ogata, H. Yoshimatsu, M. Mihara, I. Koshima, Indocyanine green lymphography findings in limb lymphedema, J. Reconstr. Microsurg. 32 (2016) 72–79.
[54] M. Mihara, H. Hara, J. Araki, K. Kikuchi, M. Narushima, T. Yamamoto, T. Iida, H. Yoshimatsu, N. Murai, K. Mitsui, T. Okitsu, I. Koshima, Indocyanine green (ICG) lymphography is superior to lymphoscintigraphy for diagnostic imaging of early lymphedema of the upper limbs, PLoS One 7 (2012), e38182.
[55] S. Akita, R. Nakamura, N. Yamamoto, H. Tokumoto, T. Ishigaki, Y. Yamaji, Y. Sasahara, Y. Kubota, N. Mitsukawa, K. Satoh, Early detection of lymphatic disorder and treatment for lymphedema following breast cancer, Plast. Reconstr. Surg. 138 (2016) 192e–202e.
[56] T. Yamamoto, H. Yoshimatsu, N. Yamamoto, Complete lymph flow reconstruction: a free vascularized lymph node true perforator flap transfer with efferent lymphaticolymphatic anastomosis, J. Plast. Reconstr. Aesthet. Surg. 69 (2016) 1227–1233.
[57] E. Farias-Cisneros, P.M. Chilton, M.D. Palazzo, T. Ozyurekoglu, J.B. Hoying, S.K. Williams, C. Baughman, C.M. Jones, C.L. Kaufman, Infrared imaging of lymphatic function in the upper extremity of normal controls and hand transplant recipients via subcutaneous indocyanine green injection, SAGE Open Med. 7 (2019) 1–12.
[58] R.M. Garza, D.W. Chang, Lymphovenous bypass for the treatment of lymphedema, J. Surg. Oncol. 118 (2018) 743–749.
[59] H. Hara, M. Mihara, Multi-area lymphaticovenous anastomosis with multi-lymphosome injection in indocyanine green lymphography: a prospective study, Microsurg 39 (2019) 167–173.
[60] P. Burnier, J. Niddam, R. Bosc, B. Hersant, J.P. Meningaud, Indocyanine green applications in plastic surgery: a review of the literature, J. Plast. Reconstr. Aesthet. Surg. 70 (2017) 814–827.
[61] S. Hameed, H. Chen, M. Irfan, S.Z. Bajwa, W.S. Khan, S.M. Baig, Z. Dai, Fluorescence guided sentinel lymph node mapping: from current molecular probes to future multimodal nanoprobes, Bioconjug. Chem. 30 (2019) 13–28.
[62] P. Soergel, H. Hertel, A.K. Nacke, R. Klapdor, T. Derlin, P. Hillemanns, Sentinel lymphadenectomy in vulvar cancer using near-infrared fluorescence from indocyanine green compared with technetium 99m nanocolloid, Int. J. Gynecol. Cancer 27 (2017) 805–812.
[63] E.C. Rossi, L.D. Kowalski, J. Scalici, L. Cantrell, K. Schuler, R.K. Hanna, M. Method, M. Ade, A. Ivanova, J.F. Boggess, A comparison of sentinel lymph node biopsy to lymphadenectomy for endometrial cancer staging (FIRES trial): a multicentre, prospective, cohort study, Lancet Oncol. 18 (2017) 384–392.
[64] C.R. Pameijer, A. Leung, R.I. Neves, J. Zhu, Indocyanine green and fluorescence lymphangiography for sentinel node identification in patients with melanoma, Am. J. Surg. 216 (2018) 558–561.
[65] L. Sorrentino, A. Sartani, G. Pietropaolo, D. Bossi, S. Mazzucchelli, M. Truffi, D. Foschi, F. Corsi, A novel indocyanine green fluorescence-guided video-assisted technique for sentinel node biopsy in breast cancer, World J. Surg. 42 (2018) 2815–2824.
[66] L.M. Mitsumori, E.S. McDonald, G.J. Wilson, P.C. Neligan, S. Minoshima, J.H. Maki, MR lymphangiography: how I do it, J. Magn. Reson. Imaging 42 (2015) 1465–1477.
[67] A.A. Gashev, T. Nagai, E.A. Bridenbaugh, Indocyanine green and lymphatic imaging: current problems, Lymphat. Res. Biol. 8 (2010) 127–130.
[68] L.M. Mitsumori, E.S. McDonald, P.C. Neligan, J.H. Maki, Peripheral magnetic resonance lymphangiography: techniques and applications, Tech. Vasc. Interv. Radiol. 19 (2016) 262–272.
[69] M.A. Mazzei, F. Gentili, F.G. Mazzei, P. Gennaro, D. Guerrieri, A. Nigri, G. Gabriele, E. Weber, A. Fausto, G. Botta, L. Volterrani, High-resolution MR lymphangiography for planning lymphaticovenous anastomosis treatment: a single-Centre experience, Radiol. Med. 122 (2017) 918–927.
[70] A.A. Zeltzer, C. Brussaard, M. Koning, R. De Baerdemaeker, B. Hendrickx, M. Hamdi, J. de Mey, MR lymphography in patients with upper limb lymphedema: the GPS for feasibility and surgical planning for lympho-venous bypass, J. Surg. Oncol. 118 (2018) 407–415.
[71] P.C. Neligan, T.A. Kung, J.H. Maki, MR lymphangiography in the treatment of lymphedema, J. Surg. Oncol. 115 (2017) 18–22.
[72] C. Lohrmann, E. Foeldi, J.P. Bartholomae, M. Langer, Gaclotericlol for MR imaging of lymphatic vessels in lymphoedematous patients: initial experience after intracutaneous injection, Br. J. Radiol. 80 (2007) 569–573.
[73] M. Borri, M.A. Schmidt, K.D. Gordon, T.A. Wallace, J.C. Hughes, E.D. Scurr, M.O. Leach, P.S. Mortimer, Quantitative contrast-enhanced magnetic resonance lymphangiography of the upper limbs in breast Cancer related lymphedema: an exploratory study, Lymphat. Res. Biol. 13 (2015) 100–106.
[74] Y. Dori, Novel lymphatic imaging techniques, Tech. Vasc. Interv. Radiol. 19 (2016) 255–261.
[75] S. Pimpalwar, P. Chinnadurai, A. Chau, M. Pereyra, D. Ashton, P. Masand, R. Krishnamurthy, S. Jadhav, Dynamic contrast enhanced magnetic resonance lymphangiography: categorization of imaging findings and correlation with patient management, Eur. J. Radiol. 101 (2018) 129–135.
[76] R. Krishnamurthy, A. Hernandez, S. Kavuk, A. Annam, S. Pimpalwar, Imaging the central conducting lymphatics: initial experience with dynamic MR lymphangiography, Radiology 274 (2015) 871–878.
[77] C.C. Pieper, H.H. Schild, Interstitial transpedal MR-lymphangiography of central lymphatics esing a standard MR contrast agent: feasibility and initial results in patients with chylous effusions, Rofo 190 (2018) 938–945.
[78] M. Cellina, G. Oliva, A. Menozzi, M. Soresina, C. Martinenghi, D. Gibelli, Non-contrast magnetic resonance lymphangiography: an emerging technique for the study of lymphedema, Clin. Imaging 53 (2019) 126–133.
[79] L. Arrive, S. Derhy, C. Dlimi, S. El Mouhadi, L. Monnier-Cholley, C. Becker, Noncontrast magnetic resonance lymphography for evaluation of lymph node transfer for secondaryupper limb lymphedema, Plast. Reconstr. Surg. 140 (2017) 806e–811e.
[80] D.X. Yu, X.X. Ma, Q. Wang, Y. Zhang, C.F. Li, Morphological changes of the thoracic duct and accessory lymphatic channels in patients with chylothorax: detection with unenhanced magnetic resonance imaging, Eur. Radiol. 23 (2013) 702–711.
[81] E.Y. Kim, H.S. Hwang, H.Y. Lee, J.H. Cho, H.K. Kim, K.S. Lee, Y.M. Shim, J. Zo, Anatomic and functional evaluation of central lymphatics with noninvasive magnetic resonance lymphangiography, Medicine 95 (2016) 1–8.
[82] L. Arrive, S. Derhy, S. El Mouhadi, L. Monnier-Cholley, Y. Menu, C. Becker, Noncontrast magnetic resonance lymphography, J. Reconstr. Microsurg. 32 (2016) 80–86.
[83] S. Rane, P.M. Donahue, T. Towse, S. Ridner, M. Chappell, J. Jordi, J. Gore, M.J. Donahue, Clinical feasibility of noninvasive visualization of lymphatic flow with

Please cite this article as: A.K. Polomska and S.T. Proulx, Imaging technology of the lymphatic system, Adv. Drug Deliv. Rev., https://doi.org/10.1016/j.addr.2020.08.013

ARTICLE IN PRESS

principles of spin labeling MR imaging: implications for lymphedema assessment, Radiology 269 (2013) 893–902.
[84] R. Crescenzi, P.M.C. Donahue, H. Mahany, S.K. Lants, M.J. Donahue, CEST MRI quantification procedures for breast cancer treatment-related lymphedema therapy evaluation, Magn. Reson. Med. 83 (2020) 1760–1773.
[85] M.J. Donahue, P.C. Donahue, S. Rane, C.R. Thompson, M.K. Strother, A.O. Scott, S.A. Smith, Assessment of lymphatic impairment and interstitial protein accumulation in patients with breast cancer treatment-related lymphedema using CEST MRI, Magn. Reson. Med. 75 (2016) 345–355.
[86] S. Hudack, P.D. McMaster, The permeability of the wall of the lymphatic capillary, J. Exp. Med. 56 (1932) 223–U225.
[87] J.M. Yoffey, C.K. Drinker, The lymphatic pathway from the nose and pharynx - the absorption of dyes, J. Exp. Med. 68 (1938) 629–U620.
[88] M.I. Harrell, B.M. Iritani, A. Ruddell, Tumor-induced sentinel lymph node lymphangiogenesis and increased lymph flow precede melanoma metastasis, Am. J. Pathol. 170 (2007) 774–786.
[89] Y. Niki, M. Ogawa, R. Makiura, Y. Magata, C. Kojima, Optimization of dendrimer structure for sentinel lymph node imaging: effects of generation and terminal group, Nanomed-Nanotechnol 11 (2015) 2119–2127.
[90] S.T. Proulx, P. Luciani, A. Christiansen, S. Karaman, K.S. Blum, M. Rinderknecht, J.C. Leroux, M. Detmar, Use of a PEG-conjugated bright near-infrared dye for functional imaging of rerouting of tumor lymphatic drainage after sentinel lymph node metastasis, Biomaterials 34 (2013) 5128–5137.
[91] A.K. Polomska, S.T. Proulx, D. Brambilla, D. Fehr, M. Bonmarin, S. Brandli, M. Meboldt, C. Steuer, T. Vasileva, N. Reinke, J.C. Leroux, M. Detmar, Minimally invasive method for the point-of-care quantification of lymphatic vessel function, JCI Insight 4 (2019) 1–16.
[92] P. Zbyszynski, I. Toraason, L. Repp, G.S. Kwon, Probing the subcutaneous absorption of a PEGylated FUD peptide nanomedicine via in vivo fluorescence imaging, Nano. Converg. 6 (2019) 22.
[93] N.A. Rohner, S.N. Thomas, Flexible macromolecule versus rigid particle retention in the injected skin and accumulation in draining lymph nodes are differentially influenced by hydrodynamic size, ACS Biomater. Sci. Eng. 3 (2017) 153–159.
[94] N.L. Trevaskis, L.M. Kaminskas, C.J. Porter, From sewer to saviour - targeting the lymphatic system to promote drug exposure and activity, Nat. Rev. Drug Discov. 14 (2015) 781–803.
[95] A. Schudel, D.M. Francis, S.N. Thomas, Material design for lymph node drug delivery, Nat. Rev. Mater. 4 (2019) 415–428.
[96] Z. Yang, R. Tian, J.J. Wu, Q.L. Fan, B.C. Yung, G. Niu, O. Jacobson, Z.T. Wang, G. Liu, G.C. Yu, W. Huang, J.B. Song, X.Y. Chen, Impact of semiconducting perylene diimide nanoparticle size on lymph node mapping and cancer imaging, ACS Nano 11 (2017) 4247–4255.
[97] X. Yang, Z. Wang, F. Zhang, G. Zhu, J. Song, G.J. Teng, G. Niu, X. Chen, Mapping sentinel lymph node metastasis by dual-probe optical imaging, Theranostics 7 (2017) 153–163.
[98] A.V. DSouza, K. Marra, J.R. Gunn, K.S. Samkoe, B.W. Pogue, Optical tracer size differences allow quantitation of active pumping rate versus stokes-Einstein diffusion in lymphatic transport, J. Biomed. Opt. 21 (2016) 100501.
[99] J.C. Kraft, P.M. Treuting, R.J.Y. Ho, Indocyanine green nanoparticles undergo selective lymphatic uptake, distribution and retention and enable detailed mapping of lymph vessels, nodes and abnormalities, J. Drug Target. 26 (2018) 494–504.
[100] S.T. Proulx, P. Luciani, S. Derzsi, M. Rinderknecht, V. Mumprecht, J.C. Leroux, M. Detmar, Quantitative imaging of lymphatic function with liposomal indocyanine green, Cancer Res. 70 (2010) 7053–7062.
[101] S. Bisso, A. Degrassi, D. Brambilla, J.C. Leroux, Poly(ethylene glycol)-alendronate coated nanoparticles for magnetic resonance imaging of lymph nodes, J. Drug Target. 27 (2019) 659–669.
[102] D. Brambilla, S.T. Proulx, P. Marschalkova, M. Detmar, J.C. Leroux, Microneedles for the noninvasive structural and functional assessment of dermal lymphatic vessels, Small 12 (2016) 1053–1061.
[103] W.J. Zhang, S.C. Song, H.X. Wang, Q. Wang, D. Li, S.Z. Zheng, Z.Y. Xu, H.T. Zhang, J. Wang, J. Sun, In vivo irreversible albumin-binding near-infrared dye conjugate as a naked-eye and fluorescence dual-mode imaging agent for lymph node tumor metastasis diagnosis, Biomaterials 217 (2019).
[104] S.T. Proulx, P. Luciani, A. Alitalo, V. Mumprecht, A.J. Christiansen, R. Huggenberger, J.C. Leroux, M. Detmar, Non-invasive dynamic near-infrared imaging and quantification of vascular leakage in vivo, Angiogenesis 16 (2013) 525–540.
[105] S.B. Bachmann, M. Detmar, S.T. Proulx, Visualization and measurement of lymphatic function in vivo, Methods Mol. Biol. 1846 (2018) 197–211.
[106] A.L. Antaris, H. Chen, K. Cheng, Y. Sun, G. Hong, C. Qu, S. Diao, Z. Deng, X. Hu, B. Zhang, X. Zhang, O.K. Yaghi, Z.R. Alamparambil, X. Hong, Z. Cheng, H. Dai, A small-molecule dye for NIR-II imaging, Nat. Mater. 15 (2016) 235–242.
[107] H.S. Park, S.H. Nam, J. Kim, H.S. Shin, Y.D. Suh, K.S. Hong, Clear-cut observation of clearance of sustainable upconverting nanoparticles from lymphatic system of small living mice, Sci. Rep. 6 (2016) 27407.
[108] M. Helle, E. Rampazzo, M. Monchanin, F. Marchal, F. Guillemin, S. Bonacchi, F. Salis, L. Prodi, L. Bezdetnaya, Surface chemistry architecture of silica nanoparticles determine the efficiency of in vivo fluorescence lymph node mapping, ACS Nano 7 (2013) 8645–8657.
[109] A.S. Cordeiro, J. Crecente-Campo, B.L. Bouzo, S.F. Gonzalez, M. de la Fuente, M.J. Alonso, Engineering polymeric nanocapsules for an efficient drainage and biodistribution in the lymphatic system, J. Drug Target. 27 (2019) 646–658.
[110] J.J. Norman, J. Gupta, S.R. Patel, S. Park, C. Jarrahian, D. Zehrung, M.R. Prausnitz, Reliability and accuracy of intradermal injection by Mantoux technique, hypodermic needle adapter, and hollow microneedle in pigs, Drug Deliv. Transl. Res. 4 (2014) 126–130.
[111] M.R. Prausnitz, Engineering microneedle patches for vaccination and drug delivery to skin, Annu. Rev. Chem. Biomol. Eng. 8 (2017) 177–200.
[112] Y. Levin, E. Kochba, I. Hung, R. Kenney, Intradermal vaccination using the novel microneedle device MicronJet600: past, present, and future, Human Vacc. Immunotherap. 11 (2015) 991–997.
[113] S. Babity, M. Roohnikan, D. Brambilla, Advances in the design of transdermal microneedles for diagnostic and monitoring applications, Small 14 (2018), e1803186.
[114] Y. Levin, E. Kochba, R. Kenney, Clinical evaluation of a novel microneedle device for intradermal delivery of an influenza vaccine: are all delivery methods the same? Vaccine 32 (2014) 4249–4252.
[115] S. Kwon, F.C. Velasquez, J.C. Rasmussen, M.R. Greives, K.D. Turner, J.R. Morrow, W.J. Hwu, R.F. Ross, S. Zhang, E.M. Sevick-Muraca, Nanotopography-based lymphatic delivery for improved anti-tumor responses to checkpoint blockade immunotherapy, Theranostics 9 (2019) 8332–8343.
[116] B. Misselwitz, MR contrast agents in lymph node imaging, Eur. J. Radiol. 58 (2006) 375–382.
[117] Y. Hama, M. Bernardo, C.A.S. Regino, Y. Koyama, M.W. Brechbiel, M.C. Krishna, P.L. Choyke, H. Kobayashi, MR lymphangiography using dendrimer-based contrast agents: a comparison at 1.5T and 3.0T, Magn. Reson. Med. 57 (2007) 431–436.
[118] Y. Koyama, V.S. Talanov, M. Bernardo, Y. Hama, C.A.S. Regino, M.W. Brechbiel, P.L. Choyke, H. Kobayashi, A dendrimer-based nanosized contrast agent, dual-labeled for magnetic resonance and optical fluorescence imaging to localize the sentinel lymph node in mice, J. Magn. Reson. Imaging 25 (2007) 866–871.
[119] R. Mounzer, P. Shkarin, X. Papademetris, T. Constable, N.H. Ruddle, T.M. Fahmy, Dynamic imaging of lymphatic vessels and lymph nodes using a bimodal nanoparticulate contrast agent, Lymphat. Res. Biol. 5 (2007) 151–158.
[120] A.C. Opina, K.J. Wong, G.L. Griffiths, B.I. Turkbey, M. Bernardo, T. Nakajima, H. Kobayashi, P.L. Choyke, O. Vasalatiy, Preparation and long-term biodistribution studies of a PAMAM dendrimer G5-Gd-BnDOTA conjugate for lymphatic imaging, Nanomedicine-Uk 10 (2015) 1423–1437.
[121] A. Ruddell, M.I. Harrell, S. Minoshima, K.R. Maravilla, B.M. Iritani, S.W. White, S.C. Partridge, Dynamic contrast-enhanced magnetic resonance imaging of tumor-induced lymph flow, Neoplasia 10 (2008) 706–713701 p following 713.
[122] A. Ruddell, S.B. Kirschbaum, S.N. Ganti, C.L. Liu, R.R. Sun, S.C. Partridge, Tumor-induced alterations in lymph node lymph drainage identified by contrast-enhanced MRI, J. Magn. Reson. Imaging 42 (2015) 145–152.
[123] S.C. Partridge, B.F. Kurland, C.L. Liu, R.J.Y. Ho, A. Ruddell, Tumor-induced lymph node alterations detected by MRI lymphography using gadolinium nanoparticles, Sci. Rep-Uk 5 (2015) 1–14.
[124] A. Muller, P. Fries, B. Jelvani, F. Lux, C.E. Rube, S. Kremp, P. Giovanoli, A. Buecker, M.D. Menger, M.W. Laschke, F.S. Frueh, Magnetic resonance lymphography at 9.4 T using a gadolinium-based nanoparticle in rats. Investigations in healthy animals and in a hindlimb lymphedema model, Investig. Radiol. 52 (2017) 725–733.
[125] J.G. McComb, Recent research into the nature of cerebrospinal fluid formation and absorption, J. Neurosurg. 59 (1983) 369–383.
[126] L. Koh, A. Zakharov, M. Johnston, Integration of the subarachnoid space and lymphatics: is it time to embrace a new concept of cerebrospinal fluid absorption? Cerebrospinal Fluid Res. 2 (2005) 6.
[127] M.E. Pizzo, D.J. Wolak, N.N. Kumar, E. Brunette, C.L. Brunnquell, M.J. Hannocks, N.J. Abbott, M.E. Meyerand, L. Sorokin, D.B. Stanimirovic, R.G. Thorne, Intrathecal antibody distribution in the rat brain: surface diffusion, perivascular transport and osmotic enhancement of delivery, J. Physiol. 596 (2018) 445–475.
[128] J.H. Ahn, H. Cho, J.H. Kim, S.H. Kim, J.S. Ham, I. Park, S.H. Suh, S.P. Hong, J.H. Song, Y.K. Hong, Y. Jeong, S.H. Park, G.Y. Koh, Meningeal lymphatic vessels at the skull base drain cerebrospinal fluid, Nature 572 (2019) 62–66.
[129] C. Gakuba, T. Gaberel, S. Goursaud, J. Bourges, C. Di Palma, A. Quenault, S.M. de Lizarrondo, D. Vivien, M. Gauberti, General anesthesia inhibits the activity of the "glymphatic system", Theranostics 8 (2018) 710–722.
[130] Q. Ma, F. Schlegel, S.B. Bachmann, H. Schneider, Y. Decker, M. Rudin, M. Weller, S.T. Proulx, M. Detmar, Lymphatic outflow of cerebrospinal fluid is reduced in glioma, Sci. Rep. 9 (2019) 14815.
[131] Q. Ma, Y. Decker, A. Müller, B.V. Ineichen, S.T. Proulx, Clearance of cerebrospinal fluid from the sacral spine through lymphatic vessels, J. Exp. Med. 216 (2019) 2492–2502.
[132] Q. Ma, B.V. Ineichen, M. Detmar, S.T. Proulx, Outflow of cerebrospinal fluid is predominantly through lymphatic vessels and is reduced in aged mice, Nat. Commun. 8 (2017) 1434.
[133] S. Da Mesquita, A. Louveau, A. Vaccari, I. Smirnov, R.C. Cornelison, K.M. Kingsmore, C. Contarino, S. Onengut-Gumuscu, E. Farber, D. Raper, K.E. Viar, R.D. Powell, W. Baker, N. Dabhi, R. Bai, R. Cao, S. Hu, S.S. Rich, J.M. Munson, M.B. Lopes, C.C. Overall, S.T. Acton, J. Kipnis, Functional aspects of meningeal lymphatics in ageing and Alzheimer's disease, Nature 560 (2018) 185–191.
[134] M. Hsu, A. Rayasam, J.A. Kijak, Y.H. Choi, J.S. Harding, S.A. Marcus, W.J. Karpus, M. Sandor, Z. Fabry, Neuroinflammation-induced lymphangiogenesis near the cribriform plate contributes to drainage of CNS-derived antigens and immune cells, Nat. Commun. 10 (2019) 1–14.
[135] E. Song, T.Y. Mao, H.P. Dong, L.S.B. Boisserand, S. Antila, M. Bosenberg, K. Alitalo, J.L. Thomas, A. Iwasaki, VEGF-C-driven lymphatic drainage enables immunosurveillance of brain tumours, Nature 577 (2020) 689−+.
[136] V. Mumprecht, M. Honer, B. Vigl, S.T. Proulx, E. Trachsel, M. Kaspar, N.E. Banziger-Tobler, R. Schibli, D. Neri, M. Detmar, In vivo imaging of inflammation- and tumor-induced lymph node lymphangiogenesis by immuno-positron emission tomography, Cancer Res. 70 (2010) 8842–8851.
[137] D.L.J. Thorek, D.S. Abou, B.J. Beattie, R.M. Bartlett, R.M. Huang, P.B. Zanzonico, J. Grimm, Positron lymphography: multimodal, high-resolution, dynamic mapping

Please cite this article as: A.K. Polomska and S.T. Proulx, Imaging technology of the lymphatic system, Adv. Drug Deliv. Rev., https://doi.org/10.1016/j.addr.2020.08.013

and resection of lymph nodes after intradermal injection of F-18-FDG, J. Nucl. Med. 53 (2012) 1438–1445.
[138] D.L.J. Thorek, D. Ulmert, N.F.M. Diop, M.E. Lupu, M.G. Doran, R.M. Huang, D.S. Abou, S.M. Larson, J. Grimm, Non-invasive mapping of deep-tissue lymph nodes in live animals using a multimodal PET/MRI nanoparticle, Nat. Commun. 5 (2014) 3097.
[139] X.L. Huang, F. Zhang, S. Lee, M. Swierczewska, D.O. Kiesewetter, L.X. Lang, G.F. Zhang, L. Zhu, H.K. Gao, H.S. Choi, G. Niu, X.Y. Chen, Long-term multimodal imaging of tumor draining sentinel lymph nodes using mesoporous silica-based nanoprobes, Biomaterials 33 (2012) 4370–4378.
[140] Y. Wang, L.X. Lang, P. Huang, Z. Wang, O. Jacobson, D.O. Kiesewetter, I.U. Ali, G.J. Teng, G. Niu, X.Y. Chen, In vivo albumin labeling and lymphatic imaging, Proc. Natl. Acad. Sci. U. S. A. 112 (2015) 208–213.
[141] A.J. Leu, D.A. Berk, F. Yuan, R.K. Jain, Flow velocity in the superficial lymphatic network of the mouse tail, Am. J. Phys. 267 (1994) H1507–H1513.
[142] M.A. Swartz, A. Kaipainen, P.A. Netti, C. Brekken, Y. Boucher, A.J. Grodzinsky, R.K. Jain, Mechanics of interstitial-lymphatic fluid transport: theoretical foundation and experimental validation, J. Biomech. 32 (1999) 1297–1307.
[143] A.J. Leu, D.A. Berk, A. Lymboussaki, K. Alitalo, R.K. Jain, Absence of functional lymphatics within a murine sarcoma: a molecular and functional evaluation, Cancer Res. 60 (2000) 4324–4327.
[144] T.P. Padera, A. Kadambi, E. di Tomaso, C.M. Carreira, E.B. Brown, Y. Boucher, N.C. Choi, D. Mathisen, J. Wain, E.J. Mark, L.L. Munn, R.K. Jain, Lymphatic metastasis in the absence of functional intratumor lymphatics, Science 296 (2002) 1883–1886.
[145] N. Isaka, T.P. Padera, J. Hagendoorn, D. Fukumura, R.K. Jain, Peritumor lymphatics induced by vascular endothelial growth factor-C exhibit abnormal function, Cancer Res. 64 (2004) 4400–4404.
[146] T. Hoshida, N. Isaka, J. Hagendoorn, E. di Tomaso, Y.L. Chen, B. Pytowski, D. Fukumura, T.P. Padera, R.K. Jain, Imaging steps of lymphatic metastasis reveals that vascular endothelial growth factor-C increases metastasis by increasing delivery of cancer cells to lymph nodes: therapeutic implications, Cancer Res. 66 (2006) 8065–8075.
[147] M. Jeltsch, A. Kaipainen, V. Joukov, X.J. Meng, M. Lakso, H. Rauvala, M. Swartz, D. Fukumura, R.K. Jain, K. Alitalo, Hyperplasia of lymphatic vessels in VEGF-C transgenic mice, Science 276 (1997) 1423–1425.
[148] T. Veikkola, L. Jussila, T. Makinen, T. Karpanen, M. Jeltsch, T.V. Petrova, H. Kubo, G. Thurston, D.M. McDonald, M.G. Achen, S.A. Stacker, K. Alitalo, Signalling via vascular endothelial growth factor receptor-3 is sufficient for lymphangiogenesis in transgenic mice, EMBO J. 20 (2001) 1223–1231.
[149] T.V. Petrova, T. Karpanen, C. Norrmen, R. Mellor, T. Tamakoshi, D. Finegold, R. Ferrell, D. Kerjaschki, P. Mortimer, S. Yla-Herttuala, N. Miura, K. Alitalo, Defective valves and abnormal mural cell recruitment underlie lymphatic vascular failure in lymphedema distichiasis, Nat. Med. 10 (2004) 974–981.
[150] I. Choi, H.K. Chung, S. Ramu, H.N. Lee, K.E. Kim, S. Lee, J. Yoo, D. Choi, Y.S. Lee, B. Aguilar, Y.K. Hong, Visualization of lymphatic vessels by Prox1-promoter directed GFP reporter in a bacterial artificial chromosome-based transgenic mouse, Blood 117 (2011) 362–365.
[151] C.F. Calvo, R.H. Fontaine, J. Soueid, T. Tammela, T. Makinen, C. Alfaro-Cervello, F. Bonnaud, A. Miguez, L. Benhaim, Y. Xu, M.J. Barallobre, I. Moutkine, J. Lyytikka, T. Tatlisumak, B. Pytowski, B. Zalc, W. Richardson, N. Kessaris, J.M. Garcia-Verdugo, K. Alitalo, A. Eichmann, J.L. Thomas, Vascular endothelial growth factor receptor 3 directly regulates murine neurogenesis, Genes Dev. 25 (2011) 831–844.
[152] R. Hagerling, C. Pollmann, L. Kremer, V. Andresen, F. Kiefer, Intravital two-photon microscopy of lymphatic vessel development and function using a transgenic Prox1 promoter-directed mOrange2 reporter mouse, Biochem. Soc. Trans. 39 (2011) 1674–1681.
[153] L.A. Truman, K.L. Bentley, E.C. Smith, S.A. Massaro, D.G. Gonzalez, A.M. Haberman, M. Hill, D. Jones, W. Min, D.S. Krause, N.H. Ruddle, ProxTom lymphatic vessel reporter mice reveal Prox1 expression in the adrenal medulla, megakaryocytes, and platelets, Am. J. Pathol. 180 (2012) 1715–1725.
[154] R. Bianchi, A. Teijeira, S.T. Proulx, A.J. Christiansen, C.D. Seidel, T. Rulicke, T. Makinen, R. Hagerling, C. Halin, M. Detmar, A transgenic Prox1-Cre-tdTomato reporter mouse for lymphatic vessel research, PLoS One 10 (2015) e0122976.
[155] M. Francois, K. Short, G.A. Secker, A. Combes, Q. Schwarz, T.L. Davidson, I. Smyth, Y.K. Hong, N.L. Harvey, P. Koopman, Segmental territories along the cardinal veins generate lymph sacs via a ballooning mechanism during embryonic lymphangiogenesis in mice, Dev. Biol. 364 (2012) 89–98.
[156] R. Hagerling, C. Pollmann, M. Andreas, C. Schmidt, H. Nurmi, R.H. Adams, K. Alitalo, V. Andresen, S. Schulte-Merker, F. Kiefer, A novel multistep mechanism for initial lymphangiogenesis in mouse embryos based on ultramicroscopy, EMBO J. 32 (2013) 629–644.
[157] I. Martinez-Corral, D. Olmeda, R. Dieguez-Hurtado, T. Tammela, K. Alitalo, S. Ortega, In vivo imaging of lymphatic vessels in development, wound healing, inflammation, and tumor metastasis, Proc. Natl. Acad. Sci. U. S. A. 109 (2012) 6223–6228.
[158] S. Kim, Y.T. Lim, E.G. Soltesz, A.M. De Grand, J. Lee, A. Nakayama, J.A. Parker, T. Mihaljevic, R.G. Laurence, D.M. Dor, L.H. Cohn, M.G. Bawendi, J.V. Frangioni, Near-infrared fluorescent type II quantum dots for sentinel lymph node mapping, Nat. Biotechnol. 22 (2004) 93–97.
[159] H. Kobayashi, Y. Hama, Y. Koyama, T. Barrett, C.A. Regino, Y. Urano, P.L. Choyke, Simultaneous multicolor imaging of five different lymphatic basins using quantum dots, Nano Lett. 7 (2007) 1711–1716.
[160] J.A. Fitzpatrick, S.K. Andreko, L.A. Ernst, A.S. Waggoner, B. Ballou, M.P. Bruchez, Long-term persistence and spectral blue shifting of quantum dots in vivo, Nano Lett. 9 (2009) 2736–2741.
[161] R. Sharma, W. Wang, J.C. Rasmussen, A. Joshi, J.P. Houston, K.E. Adams, A. Cameron, S. Ke, S. Kwon, M.E. Mawad, E.M. Sevick-Muraca, Quantitative imaging of lymph function, Am. J. Physiol. Heart Circ. Physiol. 292 (2007) H3109–H3118.
[162] S. Kwon, E.M. Sevick-Muraca, Noninvasive quantitative imaging of lymph function in mice, Lymphat. Res. Biol. 5 (2007) 219–231.
[163] Q. Zhou, R. Wood, E.M. Schwarz, Y.J. Wang, L. Xing, Near-infrared lymphatic imaging demonstrates the dynamics of lymph flow and lymphangiogenesis during the acute versus chronic phases of arthritis in mice, Arthritis Rheum. 62 (2010) 1881–1889.
[164] S. Ohnishi, S.J. Lomnes, R.G. Laurence, A. Gogbashian, G. Mariani, J.V. Frangioni, Organic alternatives to quantum dots for intraoperative near-infrared fluorescent sentinel lymph node mapping, Mol. Imaging 4 (2005) 172–181.
[165] H. Mok, H. Jeong, S.J. Kim, B.H. Chung, Indocyanine green encapsulated nanogels for hyaluronidase activatable and selective near infrared imaging of tumors and lymph nodes, Chem. Commun. 48 (2012) 8628–8630.
[166] M. Weiler, T. Kassis, J.B. Dixon, Sensitivity analysis of near-infrared functional lymphatic imaging, J. Biomed. Opt. 17 (2012) 066019-1–066019-11.
[167] M. Weiler, J.B. Dixon, Differential transport function of lymphatic vessels in the rat tail model and the long-term effects of Indocyanine Green as assessed with near-infrared imaging, Front. Physiol. 4 (2013) 1–10.
[168] T.S. Nelson, R.E. Akin, M.J. Weiler, T. Kassis, J.A. Kornuta, J.B. Dixon, Minimally invasive method for determining the effective lymphatic pumping pressure in rats using near-infrared imaging, Am. J. Physiol. Reg. I 306 (2014) R281–R290.
[169] S.T. Proulx, P. Luciani, A. Alitalo, V. Mumprecht, A.J. Christiansen, R. Huggenberger, J.C. Leroux, M. Detmar, Non-invasive dynamic near-infrared imaging and quantification of vascular leakage in vivo, Angiogenesis 16 (3) (2013) 525–540, https://doi.org/10.1007/s10456-013-9332-2.
[170] K.S. Blum, S.T. Proulx, P. Luciani, J.C. Leroux, M. Detmar, Dynamics of lymphatic regeneration and flow patterns after lymph node dissection, Breast Cancer Res. Tr 139 (2013) 81–86.
[171] E. Gousopoulos, S.T. Proulx, J. Scholl, M. Uecker, M. Detmar, Prominent lymphatic vessel hyperplasia with progressive dysfunction and distinct immune cell infiltration in lymphedema, Am. J. Pathol. 186 (2016) 2193–2203.
[172] T.S. Nelson, Z. Nepiyushchikh, J.S.T. Hooks, M.S. Razavi, T. Lewis, C.C. Clement, M. Thoresen, M.T. Cribb, M.K. Ross, R.L. Gleason, L. Santambrogio, J.F. Peroni, J.B. Dixon, Lymphatic remodelling in response to lymphatic injury in the hind limbs of sheep, Nat. Biomed. Eng. 16 (2019) 525–540.
[173] K.S. Blum, S. Karaman, S.T. Proulx, A.M. Ochsenbein, P. Luciani, J.C. Leroux, C. Wolfrum, M. Detmar, Chronic high-fat diet impairs collecting lymphatic vessel function in mice, PLoS One 9 (2014) e94713.
[174] N. Escobedo, S.T. Proulx, S. Karaman, M.E. Dillard, N. Johnson, M. Detmar, G. Oliver, Restoration of lymphatic function rescues obesity in Prox1-haploinsufficient mice, JCI Insight 1 (2016) e85096.
[175] S.T. Proulx, Q. Ma, D. Andina, J.C. Leroux, M. Detmar, Quantitative measurement of lymphatic function in mice by noninvasive near-infrared imaging of a peripheral vein, JCI Insight 2 (2017), e90861.
[176] A. Aspelund, S. Antila, S.T. Proulx, T.V. Karlsen, S. Karaman, M. Detmar, H. Wiig, K. Alitalo, A dural lymphatic vascular system that drains brain interstitial fluid and macromolecules, J. Exp. Med. 212 (2015) 991–999.
[177] S. Zackrisson, S.M.W.Y. van de Ven, S.S. Gambhir, Light in and sound out: emerging translational strategies for photoacoustic imaging, Cancer Res. 74 (2014) 979–1004.
[178] T. Vu, D. Razansky, J. Yao, Listening to tissues with new light: recent technological advances in photoacoustic imaging, J. Opt. 21 (2019) 103001.
[179] X.L. Dean-Ben, D. Razansky, Optoacoustic image formation approaches-a clinical perspective, Phys. Med. Biol. 64 (2019) 18TR01.
[180] K.H. Song, E.W. Stein, J.A. Margenthaler, L.V. Wang, Noninvasive photoacoustic identification of sentinel lymph nodes containing methylene blue in vivo in a rat model, J. Biomed. Opt. 13 (2008), 054033.
[181] D.P.J. Pan, M. Pramanik, A. Senpan, S. Ghosh, S.A. Wickline, L.V. Wang, G.M. Lanza, Near infrared photoacoustic detection of sentinel lymph nodes with gold nanobeacons, Biomaterials 31 (2010) 4088–4093.
[182] T.N. Erpelding, C. Kim, M. Pramanik, L. Jankovic, K. Maslov, Z.J. Guo, J.A. Margenthaler, M.D. Pashley, L.H.V. Wang, Sentinel lymph nodes in the rat: noninvasive photoacoustic and US imaging with a vlinical US system, Radiology 256 (2010) 102–110.
[183] C. Kim, H.M. Song, X. Cai, J.J. Yao, A. Wei, L.H.V. Wang, In vivo photoacoustic mapping of lymphatic systems with plasmon-resonant nanostars, J. Mater. Chem. 21 (2011) 2841–2844.
[184] C. Martel, J.J. Yao, C.H. Huang, J. Zou, G.J. Randolph, L.V. Wang, Photoacoustic lymphatic imaging with high spatial-temporal resolution, J. Biomed. Opt. 19 (2014) 116009–1–116009–7.
[185] A. Taruttis, V. Ntziachristos, Advances in real-time multispectral optoacoustic imaging and its applications, Nat. Photonics 9 (2015) 219–227.
[186] A. Forbrich, A. Heinmiller, R.J. Zemp, Photoacoustic imaging of lymphatic pumping, J. Biomed. Opt. 22 (2017) 106003–1–106003–106006.
[187] S. Kwon, G.D. Agollah, G. Wu, E.M. Sevick-Muraca, Spatio-temporal changes of lymphatic contractility and drainage patterns following lymphadenectomy in mice, PLoS One 9 (2014) e106034.
[188] S.B. Bachmann, S.T. Proulx, Y.L. He, M. Ries, M. Detmar, Differential effects of anaesthesia on the contractility of lymphatic vessels in vivo, J. Physiol. London 597 (2019) 2841–2852.
[189] B.J. Vakoc, R.M. Lanning, J.A. Tyrrell, T.P. Padera, L.A. Bartlett, T. Stylianopoulos, L.L. Munn, G.J. Tearney, D. Fukumura, R.K. Jain, B.E. Bouma, Three-dimensional microscopy of the tumor microenvironment in vivo using optical frequency domain imaging, Nat. Med. 15 (2009) 1219–1223.
[190] Z. Zhi, Y. Jung, R.K. Wang, Label-free 3D imaging of microstructure, blood, and lymphatic vessels within tissue beds in vivo, Opt. Lett. 37 (2012) 812–814.

Please cite this article as: A.K. Polomska and S.T. Proulx, Imaging technology of the lymphatic system, Adv. Drug Deliv. Rev., https://doi.org/10.1016/j.addr.2020.08.013

ARTICLE IN PRESS

[191] S. Yousefi, J. Qin, Z.W. Zhi, R.K.K. Wang, Label-free optical lymphangiography: development of an automatic segmentation method applied to optical coherence tomography to visualize lymphatic vessels using Hessian filters, J. Biomed. Opt. 18 (2013) 086004-1–086004-9.
[192] J. Horstmann, H. Schulz-Hildebrandt, F. Bock, S. Siebelmann, E. Lankenau, G. Huttmann, P. Steven, C. Cursiefen, Label-free in vivo imaging of corneal lymphatic vessels using microscopic optical coherence tomography, Invest. Ophthalmol. Vis. Sci. 58 (2017) 5872–5878.
[193] P.J. Gong, D.Y. Yu, Q. Wang, P.K. Yu, K. Karnowski, M. Heisler, A. Francke, D. An, M.V. Sarunic, D.D. Sampson, Label-free volumetric imaging of conjunctival collecting lymphatics ex vivo by optical coherence tomography lymphangiography, J. Biophotonics 11 (2018) e201800070.
[194] S.D. Zawieja, J.A. Castorena-Gonzalez, B. Dixon, M.J. Davis, Experimental models used to assesslymphatic contractile function, Lymphat. Res. Biol. 15 (2017) 331–342.
[195] J.P. Scallan, S.D. Zawieja, J.A. Castorena-Gonzalez, M.J. Davis, Lymphatic pumping: mechanics, mechanisms and malfunction, J. Physiol. London 594 (2016) 5749–5768.
[196] D.C. Zawieja, Contractile physiology of lymphatics, Lymphat. Res. Biol. 7 (2009) 87–96.
[197] J.P. Scallan, M.J. Davis, Genetic removal of basal nitric oxide enhances contractile activity in isolated murine collecting lymphatic vessels, J. Physiol. London 591 (2013) 2139–2156.
[198] J.A. Castorena-Gonzalez, S.D. Zawieja, M. Li, R.S. Srinivasan, A.M. Simon, C. de Wit, R. de la Torre, L.A. Martinez-Lemus, G.W. Hennig, M.J. Davis, Mechanisms of connexin-related lymphedema: a critical role for Cx45, but not Cx43 or Cx47, in the entrainment of spontaneous lymphatic contractions, Circ. Res. 123 (2018) 964–985.
[199] S. Liao, G. Cheng, D.A. Conner, Y. Huang, R.S. Kucherlapati, L.L. Munn, N.H. Ruddle, R.K. Jain, D. Fukumura, T.P. Padera, Impaired lymphatic contraction associated with immunosuppression, Proc. Natl. Acad. Sci. U. S. A. 108 (2011) 18784–18789.
[200] M.J. Weiler, M.T. Cribb, Z. Nepiyushchikh, T.S. Nelson, J.B. Dixon, A novel mouse tail lymphedema model for observing lymphatic pump failure during lymphedema development, Sci. Rep-Uk 9 (2019) 10405.
[201] C. Chong, F. Scholkmann, S.B. Bachmann, P. Luciani, J.C. Leroux, M. Detmar, S.T. Proulx, In vivo visualization and quantification of collecting lymphatic vessel contractility using near-infrared imaging, Sci. Rep. 6 (2016) 22930.
[202] S.B. Bachmann, D. Gsponer, J.A. Montoya-Zegarra, M. Schneider, F. Scholkmann, C. Tacconi, S.F. Noerrelykke, S.T. Proulx, M. Detmar, A distinct role of the autonomic nervous system in modulating the function of lymphatic vessels under physiological and tumor-draining conditions, Cell Rep. 27 (2019) 3305−+.
[203] A. Gogineni, M. Caunt, A. Crow, C.V. Lee, G. Fuh, N. van Bruggen, W.L. Ye, R.M. Weimer, Inhibition of VEGF-C modulates distal lymphatic remodeling and secondary metastasis, PLoS One 8 (2013) e68755.
[204] E.M. Bouta, C. Blatter, T.A. Ruggieri, E.F.J. Meijer, L.L. Munn, B.J. Vakoc, T.P. Padera, Lymphatic function measurements influenced by contrast agent volume and body position, JCI Insight 3 (2018) e96591.
[205] C. Blatter, E.F.J. Meijer, A.S. Nam, D. Jones, B.E. Bouma, T.P. Padera, B.J. Vakoc, In vivo label-free measurement of lymph flow velocity and volumetric flow rates using Doppler optical coherence tomography, Sci. Rep-Uk 6 (2016) e68755.
[206] C. Blatter, E.F.J. Meijer, T.P. Padera, B.J. Vakoc, Simultaneous measurements of lymphatic vessel contraction, flow and valve dynamics in multiple lymphangions using optical coherence tomography, J. Biophotonics 11 (2018) 1–12 e201700017.
[207] S. Modi, A.W.B. Stanton, W.E. Svensson, A.M. Peters, P.S. Mortimer, J.R. Levick, Human lymphatic pumping measured in healthy and lymphoedematous arms by lymphatic congestion lymphoscintigraphy, J. Physiol. 583 (2007) 271–285.
[208] T. Saito, N. Unno, N. Yamamoto, K. Inuzuka, H. Tanaka, M. Sano, R. Sugisawa, K. Katahashi, H. Konno, Low lymphatic pumping pressure in the legs is associated with leg edema and lower quality of life in healthy volunteers, Lymphat. Res. Biol. 13 (2015) 154–159.
[209] N. Unno, M. Nishiyama, M. Suzuki, H. Tanaka, N. Yamamoto, D. Sagara, Y. Mano, H. Konno, A novel method of measuring human lymphatic pumping using indocyanine green fluorescence lymphography, J. Vasc. Surg. 52 (2010) 946–952.
[210] N. Unno, H. Tanaka, M. Suzuki, N. Yamamoto, Y. Mano, M. Sano, T. Saito, H. Konno, Influence of age and gender on human lymphatic pumping pressure in the leg, Lymphology 44 (2011) 113–120.
[211] M.S. Razavi, T.S. Nelson, Z. Nepiyushchikh, R.L. Gleason, J.B. Dixon, The relationship between lymphangion chain length and maximum pressure generation established through in vivo imaging and computational modeling, Am. J. Physiol. Heart C 313 (2017) H1249–H1260.
[212] T.V. Karlsen, E. McCormack, M. Mujic, O. Tenstad, H. Wiig, Minimally invasive quantification of lymph flow in mice and rats by imaging depot clearance of near-infrared albumin, Am. J. Physiol. Heart Circ. Physiol. 302 (2012) H391–H401.
[213] S. Karaman, D. Buschle, P. Luciani, J.C. Leroux, M. Detmar, S.T. Proulx, Decline of lymphatic vessel density and function in murine skin during aging, Angiogenesis 18 (2015) 489–498.
[214] T.N. Doan, F.C. Bernard, J.M. McKinney, J.B. Dixon, N.J. Willett, Endothelin-1 inhibits size dependent lymphatic clearance of PEG-based conjugates after intra-articular injection into the rat knee, Acta Biomater. 93 (2019) 270–281.
[215] Y.H. Yucel, K. Cardinell, S. Khattak, X. Zhou, M. Lapinski, F. Cheng, N. Gupta, Active lymphatic drainage from the eye measured by noninvasive photoacoustic imaging of near-infrared nanoparticles, Invest. Ophthalmol. Vis. Sci. 59 (2018) 2699–2707.
[216] M. Ionac, One technique, two approaches, and results: thoracic duct cannulation in small laboratory animals, Microsurg 23 (2003) 239–245.
[217] R. Huggenberger, S. Ullmann, S.T. Proulx, B. Pytowski, K. Alitalo, M. Detmar, Stimulation of lymphangiogenesis via VEGFR-3 inhibits chronic skin inflammation, J. Exp. Med. 207 (2010) 2255–2269.
[218] D. Tobbia, J. Semple, A. Baker, D. Dumont, A. Semple, M. Johnston, Lymphedema development and lymphatic function followinglymph node excision in sheep, J. Vasc. Res. 46 (2009) 426–434.
[219] A. Baker, J.L. Semple, S. Moore, M. Johnston, Lymphatic function is impaired following irradiation of a single lymph node, Lymphat. Res. Biol. 12 (2014) 76–88.
[220] Q. Ma, M. Ries, Y. Decker, A. Muller, C. Riner, A. Bucker, K. Fassbender, M. Detmar, S.T. Proulx, Rapid lymphatic efflux limits cerebrospinal fluid flow to the brain, Acta Neuropathol. 137 (2019) 151–165.
[221] H. Kajita, K. Kishi, High-resolution imaging of lymphatic vessels with photoacoustic lymphangiography, Radiology 292 (2019) 35.
[222] M. Kuniyil Ajith Singh, T. Agano, N. Sato, Y. Shigeta, T. Uemura, Real-time in vivo imaging of human lymphatic system using an LED-based photoacoustic/ultrasound imaging system, SPIE 10494 (2018) 1049404–1–1049404–1049406.
[223] H. Kajita, A. Oh, M. Urano, M. Takemaru, N. Imanishi, M. Otaki, T. Yagi, S. Aiso, K. Kishi, Photoacoustic lymphangiography, J. Surg. Oncol. 121 (2020) 48–50.
[224] G. Giacalone, T. Yamamoto, F. Belva, A. Hayashi, Bedside 3D visualization of lymphatic vessels with a handheld multispectral optoacoustic tomography device, J. Clin. Med. 9 (2020) 1–10.
[225] I. Stoffels, S. Morscher, I. Helfrich, U. Hillen, J. Leyh, N.C. Burton, T.C. Sardella, J. Claussen, T.D. Poeppel, H.S. Bachmann, A. Roesch, K. Griewank, D. Schadendorf, M. Gunzer, J. Klode, Metastatic status of sentinel lymph nodes in melanoma determined noninvasively with multispectral optoacoustic imaging, Sci. Transl. Med. 7 (2015)317ra199.
[226] A. Garcia-Uribe, T.N. Erpelding, A. Krumholz, H. Ke, K. Maslov, C. Appleton, J.A. Margenthaler, L.V. Wang, Dual-modality photoacoustic and ultrasound imaging system for noninvasive sentinel lymph node detection in patients with breast cancer, Sci. Rep. 5 (2015) 15748.
[227] A. Hayashi, G. Giacalone, T. Yamamoto, F. Belva, G. Visconti, N. Hayashi, M. Handa, H. Yoshimatsu, M. Salgarello, Ultra high-frequency ultrasonographic imaging with 70 MHz scanner for visualization of the lymphatic vessels, Plast Reconstr. Surg. Glob. Open 7 (2019) e2086.
[228] A. Hayashi, G. Visconti, T. Yamamoto, G. Giacalone, N. Hayashi, M. Handa, H. Yoshimatsu, M. Salgarello, Intraoperative imaging of lymphatic vessel using ultra high-frequency ultrasound, J. Plast. Reconstr. Aesthet. Surg. 71 (2018) 778–780.
[229] M. Czedik-Eysenberg, J. Steinbacher, B. Obermayer, H. Yoshimatsu, H. Hara, M. Mihara, C.J. Tzou, S. Meng, Exclusive use of ultrasound for locating optimal LVA sites-a descriptive data analysis, J. Surg. Oncol. 121 (2020) 51–56.
[230] A. Hayashi, N. Hayashi, H. Yoshimatsu, T. Yamamoto, Effective and efficient lymphaticovenular anastomosis using preoperative ultrasound detection technique of lymphatic vessels in lower extremity lymphedema, J. Surg. Oncol. 117 (2018) 290–298.
[231] A. Hayashi, T. Yamamoto, H. Yoshimatsu, N. Hayashi, M. Furuya, M. Harima, M. Narushima, I. Koshima, Ultrasound visualization of the lymphatic vessels in the lower leg, Microsurg 36 (2016) 397–401.
[232] M. Mihara, H. Hara, Y. Kawakami, Ultrasonography for classifying lymphatic sclerosis types and deciding optimal sites for lymphatic-venous anastomosis in patients with lymphoedema, J. Plast. Reconstr. Aesthet. Surg. 71 (2018) 1274–1281.
[233] M. Mihara, H. Hara, Y. Hayashi, M. Narushima, T. Yamamoto, T. Todokoro, T. Iida, N. Sawamoto, J. Araki, K. Kikuchi, N. Murai, T. Okitsu, I. Kisu, I. Koshima, Pathological steps of cancer-related lymphedema: histological changes in the collecting lymphatic vessels after lymphadenectomy, PLoS One 7 (2012) e41126.

Please cite this article as: A.K. Polomska and S.T. Proulx, Imaging technology of the lymphatic system, Adv. Drug Deliv. Rev., https://doi.org/10.1016/j.addr.2020.08.013